MASTER THESIS

TUDelft

Adsorption of Organic Micro-pollutants by Zeolite Granules: Batch and Column Studies

Rong Hu
Sep 2020

Adsorption of Organic Micro-pollutants by Zeolite Granules: Batch and Column Studies

by

Rong Hu

to obtain the degree of
Master of Science in Civil Engineering (Track of Environmental Engineering)
at the Delft University of Technology.

An electronic version of this thesis is available at http://repository.tudelft.nl/.

TUDelft

ABSTRACT

The presence of organic micro-pollutants (OMPs) has caused increasing contamination of aquatic systems. In recent years, the selective adsorption of target OMPs by zeolites have been proved efficient for OMP removal. For the potential application of zeolites in the wastewater treatment plants, zeolite granules are preferably used in order to avoid the post-filtration for zeolite powders. Therefore, the knowledge on the performance of zeolite granules for the removal of OMPs should be fully understood.

In this research, BEA and MOR zeolite granules were used as adsorbents for the removal of 11 OMPs from water, which were carbamazepine, diclofenac, 1H-benzotriazole, methyl-benzotriazole, hydrochlorothiazide, sulfamethoxazole, clarithromycin, propranolol, trimethoprim, metoprolol and sotalol. The aims of this study were: (1) to investigate the adsorption capacity and kinetics of the 11 OMPs by zeolite granules in both demineralized water and wastewater (WW), in batch experiments; (2) to predict the breakthrough curve of columns packed with zeolite granules by using a mathematical model combining the parameters determined by batch experiments.

It was found that the charge and hydrophobicity of OMPs were the two main factors that affected the adsorption capacity of OMPs by zeolites, while the effect of OMP size on the adsorption capacity was negligible. The OMP adsorption capacities by zeolite granules were less than OMP adsorption capacities by zeolite powders. The fittings of the IPD model to the adsorption kinetic data showed that film diffusion and intra-particle diffusion were both the rate-limiting steps in the adsorption of OMPs by zeolite granules. Furthermore, the adsorption capacity and rate of OMPs in WW were lower in comparison with OMP adsorption in demineralized water, which could be caused by the higher pH in WW and the pore-blocking effect by background organic matters. In the column experiments, it was found that OMP breakthrough percentage in the column was determined by both the adsorption capacity and kinetics of OMPs by zeolite granules.

In the breakthrough model, the kinetic and isotherm constants from batch experiments overestimated the adsorption rate and capacity of zeolite granules in the columns, and the overestimated isotherm constant was the main factor that caused the deviation of the model prediction. With a lower isotherm constant, the model was able to provide good resemblance between modelled and measured breakthrough curves. Furthermore, with a known breakthrough curve at a certain EBCT, the model was able to determine a proper isotherm constant, which can be used to predict the breakthrough curve at a different EBCT.

ACKNOWLEDGEMENTS

Time flies, after ten months of work, my thesis was finally finished, which also means the end of my two years in the Netherlands. Looking back at the two years, I believe that this long journey must be the most challenging, unique and precious time of my life.

These ten months were the experience fulled of ups and downs like taking a roller coaster. During the special lockdown period, everything seemed to be more difficult for everyone. However, I still received lots of help from many people. First of all, I would like to express my special thanks to my committee. Prof. Jan Peter van der Hoek, as the chair of the committee, gave me a lot of valuable suggestions on improving my report. Dr. Bas Heijman was the one who always guided me to the right track. Every time I had confusions, he was always willing to help me find the solutions. Dr. Gerrit inspired me a lot on how to explain the model results. I also want to express my thanks to my daily supervisor, Dr. Nan Jiang. When I ran into problems, she was always the first person that was happy to offer me a hand. Without her help, it would have been really hard to finish my work. Thanks to Mingyan Fu for providing me with the instructions on the experiment design and the model setting up.

I would also like to thank my friends in Delft for bringing my life so much fun and taking loneliness away from me, I feel grateful to have them in my life. At the same time, I also want to express my love and thanks to my boyfriend Jing Huang, it was his encouragement that takes me out of the dark every time. Last but not least, I would like to express my deepest love and gratitude to my parents, it is them who makes me who I am today.

I will never forget these days in Delft. I promise myself, I will be a better me when I come back again.

Rong Hu
August 20, 2020
Delft

CONTENTS

LIST OF FIGURES

LIST OF TABLES

LIST OF ABBREVIATIONS

AAS Adsorption onto active sites model.
AOP Advanced oxidation process.

BOM Background organic matter.

DBP Disinfection by-product.
Demi-water Demineralised water.

EBCT Empty bed contact time.
ECC Emerging contaminants of concern.
ESI Electrospray ionization.

F&S Frusawa and Smith mode.
FPSD Film-pore and surface diffusion mode.

GAC Granular activated carbon.

I&W Ministry of Infrastructure and Water Management.
IPD Intra-particle diffusion model.

LC-MS Liquid Chromatography–Mass Spectrometry.

MTBE Methyltertiary butyl ether.

NF Nanofiltration.

OMP Organic micro pollutant.

PDE Partial differential equation.
PFO Pseudo first order model.
PPCP Personal care products.
PSO Pseudo second order model.

RO Reverse osmosis.

WW Wastewater.
WWTP Wastewater treatment plant.

1 | INTRODUCTION

1.1 THE OCCURRENCE OF ORGANIC MICRO–POLLUTANTS

The discharge of agriculture, industry, as well as the effluent of wastewater treatment plants (WWTPs) are polluting the global water resources drastically and are reducing the availability of clean water. Among various pollutants, organic micro-pollutants (OMPs) are considered as contaminants of emerging concern. OMPs, including pharmaceuticals, personal care products, pesticides and various industrial additive, are widely detected in global aquatic environment at trace concentration level ranging from a few ng/L to several µg/L [Luo et al., 2014].

The effluent of WWTPs is an important source of OMP discharging. The conventional WWTPs are not designed to remove OMPs. OMPs that are partially removed by biological treatment will be discharged with the effluents of WWTPs into water bodies. In the Netherlands, the Ministry of Infrastructure and Water Management (I&W) has advocated the development of innovative technologies to remove OMPs from secondary effluent of WWTPs. According to the I&W, due to the common present in effluent and the poor removal in the existing WWTPs, 11 OMPs are selected as potential guide substances to clarify the performance of the purification technologies, which are carbamazepine, propranolol, trimethoprim, metoprolol, 1H-benzotriazole, methyl-benzotriazole, hydrochlorothiazide, sulfamethoxazole, diclofenac, clarithromycin and sotalol.

Loos et al. [2013] studied the removal of 156 polar OMPs in 90 European WWTPs. The median concentrations found in this EU-wide WWTP study were 2.7 µg/L for 1H-benzotriazole, 2.1 µg/L for methyl-benzotriazole, 178 ng/L for trimethoprim, 752 ng/L for carbamazepine, 43 ng/L for diclofenac and 164 ng/L for sulfmethoxazole. As a type of anti-corrosive agent, benzotriazole was reported to be with high water solubility and high polarity; meanwhile, they are of moderate persistence to the photochemical and biological degradation processes. Trimethoprim and diclofenac were shown to be poorly biodegradable and can hardly be adsorbed to sludge, resulting in low removal efficiency in biological treatment [Göbel et al., 2007; Marta et al., 2016]. Carbamazepine, sulfamethoxazole are found to be almost completely persistent during activated sludge treatment [Clara et al., 2005].

Other pharmaceuticals, such as hydrochlorothiazide, was detected in very high frequency (>85%) in concentrations ranging from 100 ng/L to 17.2 µg/L in municipal wastewater samples in the Netherlands [Oosterhuis et al., 2013], and the elimination of this compound was found to be incomplete (0–77%) during conventional biological treatment [Castiglioni et al., 2006]. Beta-blocker, such as sotalol, metoprolol and propranolol, have been used to treat human hypertension since the late 1960s [Maurer et al., 2007], they are usually present in WWTPs effluent with concentrations ranging from 10 ng/L to 1000 ng/L. Beta-blocker are known to be hardly adsorbed to the sludge in WWTPs.

The occurrence of OMPs in water body may cause consequent contamination of drinking water sources [Marta et al., 2016]. Tröger et al. [2018] applied a field study in central Sweden on water from source to tap, 41 OMPs out of 134 OMPs were found to be present in the drinking water system with individual concentrations ranging from sub ng/L levels to 80 ng/L. Despite the low concentrations, the accumulating of OMPs in aquatic systems will cause the endocrine disruption of human and aquatic animals, as well as the pathogen resistance in aquatic organisms [Gavrilescu et al., 2015]. The potential adverse effects of OMPs on human and aquatic ecosystem have aroused increasing public concern [Gavrilescu et al., 2015]. Therefore, upgrading WWTPs with tertiary or complementary treatment steps to remove OMPs from the effluent should be taken into consideration.

1.2 CURRENT TECHNOLOGIES FOR OMP REMOVAL

A range of advanced water treatment technologies such as oxidation, membrane separation and adsorption by activated carbon have been developed for the removal of OMPs from water.

1.2.1 Chemical oxidation

The existing studies demonstrated that ozonation and advanced oxidation processes (AOPs) are efficient ways for the removal of OMPs from wastewater (WW) [Katsoyiannis et al., 2011; Kruithof et al., 2006; Swaim et al., 2008]. Treatment with ozone has two different mechanisms of action. In the alkaline pH range, a radical mechanism of ozonation is characteristic, while in acidic and neutral conditions, direct reaction of ozone with organic substances usually takes place [Szabová et al., 2020]. AOPs use highly reactive hydroxyl radicals to oxidize organic pollutants. Compared to ozonation, AOPs have better oxidation ability without selectivity due to hydroxyl radicals that can react on broader types of molecules [Acero and Von Gunten, 2001]

However, as the treatment for the whole water stream is required, high energy and

oxidant consumption are needed for chemical oxidation process. Since hydroxyl radicals react non-selectively, numerous undesired by-products are formed at low concentration levels [Chiron et al., 2000].

1.2.2 Membrane separation

Membrane filtration is an efficient technology to remove OMPs from water bodies by physical separation [Kimura et al., 2003; Baresel et al., 2019]. The most widely studied membrane technologies for the removal of OMPs are nanofiltration (NF) and reverse osmosis (RO). The research done by Kimura et al. [2003] indicated that the OMP removal efficiency is affected by the charge and molecular size of OMPs. According to Laîné et al. [2003], the presence of background organic matters (BOMs) in water could cause bio-fouling of the membrane. Membrane fouling is considered a major obstacle for efficient membrane operation due to declining permeate flux, increased operational cost, and shortened membrane life [Xu et al., 2006]. In addition, concentrate disposal is another obstacle that increases the overall economic expense of a membrane plant [Squire, 2000].

1.2.3 Adsorption by activated carbon

Adsorption of OMPs by porous materials is known as one of the most effective methods to remove OMPs. Activated carbon is the most commonly used adsorbent to remove OMPs from water due to the large surface area, well-developed pore structure and a high degree of surface reactivity [Castilla, 2004], and it is a broad-spectrum agent that effectively removes a wide range of OMPs in many water supplies [Mohammad-Khah and Ansari, 2009].

However, many hydrophilic OMPs are hardly removed by activated carbon. Exhausted carbon will be regenerated or be disposed after adsorption. The thermal regenerating of activated carbon requires heating up to 900 °C [Alsbaiee et al., 2016], and thus is energy consuming. The research done by San Miguel et al. [2001] indicated that carbon loss may reach 22 % during the thermal regeneration under 800 °C. Furthermore, the presence of BOMs in the water could lower the adsorption efficiency of activated carbon for OMP removal [Jiang et al., 2018].

1.3 ZEOLITE AS ADSORBENT FOR THE REMOVAL OF OMPS
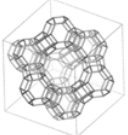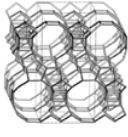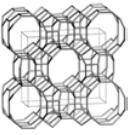
In recent years, zeolite is considered as an alternative option for the adsorption of target pollutants from water. In this section, the physicochemical properties of zeolites,

the adsorption mechanisms of OMPs by zeolite powders and the potential application of zeolite granules for the removal of OMPs will be discussed.

1.3.1 Physicochemical properties of zeolite

Zeolite is a type of crystalline aluminosilicate with 3-dimensional structure constructed by TO_4 tetrahedra (in which the T atom is either a Si^{4+} or Al^{3+} atom located in the centre of an oxygen tetrahedron) [Li and Yu, 2014]. The hydrophobicity increases with decreasing aluminium content and zeolites with higher Si/Al ratio are more hydrophobic [Damjanovi´ et al., 2010]. High-silica zeolite with Si/Al ratio up to a few thousand is beneficial to OMP adsorption from water [Tsitsishvili, 1973].

Table 1.1: Key properties of four commonly used zeolite frameworks *

Zeolite type	Framework structure [a]	Pore opening size (Å*Å) [a]	Framework density T atoms (Å^3) $^{-1}$ [a]	Maximum diameter of a sphere can be included (Å) [b]
FAU		12 rings: 7.4*7.4	12.7	11.24
BEA		12 rings: 6.6*6.7 12 rings: 5.6*5.6	15.1	6.68
MOR		12 rings: 6.5*7.4 8 rings: 2.6*5.7	17.2	6.70
MFI		10 rings: 5.1*5.5 10 rings: 5.3*5.6	17.9	6.36

* Cited from [Jiang et al., 2018]

[a] [Baerlocher et al., 2007]

[b] Maximum diameter of a sphere were calculated by Mike Treacy, Arizona State University, using his codes "TOTOPOL" and "DelaneysDonkey." [Foster et al., 2006].

The structural features of zeolite are mostly described by their framework types. The most commercially available and commonly studied framework types are FAU, BEA, MOR and MFI. The key properties of the four frameworks are presented in Table 1.1. The pore volume of zeolites would follow the order of FAU > BEA > MOR > MFI.

FAU with large pore opening size has cage structure of pore opening. However, zeolites with smaller pore opening size, such as MOR and MFI, have narrow channel pore openings [Baerlocher et al., 2007]. Due to the uniform pore size, zeolites have good efficiency and selectivity for OMP adsorption. BOMs with larger sizes than the pore size of zeolites will be excluded from adsorption [Jiang et al., 2018; Damjanoví́c et al., 2010; Zhang et al., 2016].

1.3.2 Adsorption mechanisms of OMPs by zeolite powders

Currently, most research on OMP adsorption by zeolites focused on zeolite powder in batch mode. Zeolite powders are known to be effective for the removal of a wide range of OMPs from water [De Ridder et al., 2012; Rungsirisakun et al., 2006; Rossner et al., 2009; Jiang et al., 2020]. The adsorption mechanisms of OMPs by zeolite powders have been well discussed. First of all, the adsorption efficiency of OMPs were decided by the pore size of zeolites. Due to larger van der Waals force between OMPs and zeolite surface, OMPs with molecular size similar to the zeolite pore size would have better removal efficiency, and the phenomenon is called "Close-fit" [De Ridder et al., 2012].

Secondly, the surface of zeolite is negatively charged, so the electrostatic interaction between zeolite surface and OMPs would also affect the adsorption [Auerbach et al., 2003]. It has been proved that, at the OMP concentration range from ng/L to µg/L, positively charged OMPs are better adsorbed than neutral and negatively charged OMPs by zeolites [Jiang, 2019].

Thirdly, the adsorption sites on the zeolite surface also have impacts on the adsorption of OMPs. Oxygen and acidic sites are the two main adsorption sites which might promote the adsorption of certain types of OMPs. Koubaissy et al. [2011] indicated that it can form an electron donor-acceptor complex between the hydrogen from the aromatic ring of OMPs and the oxygen site from zeolites. According to Valdés et al. [2014], OMPs with the character of weak base (e.g. toluene and benzene) can interact with Brønsted acid sites and Lewis acid sites on zeolites by forming hydrogen bonds and Lewis acid-base adducts, respectively.

1.3.3 Potential application of zeolite granules for OMP removal in water treatment

In most practical cases, suitable adsorbents are packed in columns. Water containing particular pollutants is passed through the column and pollutants will be removed [Yusuff et al., 2013]. By applying zeolite-granule packed columns, the post filtration process to remove zeolite powders from water will be avoided. Nonetheless, there are only a few publications elaborating the adsorption of OMPs by zeolite granules in column scale. Abu-Lail et al. [2010] studied the adsorption of methyl tertiary butyl ether

(MTBE) by zeolite granules. Rossner and Knappe [2008] compared the effectiveness of silicalite zeolite granules, carbonaceous resin, and coconut-shell-based granular activated carbon (GAC) for the removal of MTBE from water.

After a period of operating, the exhausted adsorbents need to be properly treated to prevent the toxic residue re-entering the environment. As a type of aluminosilicate crystal, the high stability of zeolites under oxidative conditions may ensure the regeneration of zeolites through (advanced) oxidation without compromising their surface properties and pore structure [Jiang et al., 2018]. By using zeolite granules, the chemical regeneration can be potentially combined with zeolite adsorption to fulfil the on-site adsorption-regeneration.

1.4 MATHEMATICAL MODELLING IN ADSORPTION

In the literature, the performance of adsorbents are usually described from three aspects: equilibrium and kinetics of the adsorbent, and the breakthrough curve in the adsorbent packed column. Various mathematical models have been proposed in literature regarding these three aspects. The models are used to fit the experimental data and to make predictions on the adsorbent performance.

The adsorption isotherm models describe the adsorption equilibrium between OMP concentration in liquid phase (solution) and in solid phase (adsorbent) at constant temperature and pH. The isotherm constants can be used to estimate the adsorption capacities of OMPs and to compare the adsorption efficiency of adsorbents. The most widely employed isotherm models are Langmuir [Langmuir, 1916] and Freundlich isotherms [Freundlich, 1906]. Other isotherm models such as Sips isotherm [Sips, 1948] and Redlich–Peterson isotherm [Redlich and Peterson, 1959] are also applied in the literature.

Various adsorption kinetics models have been developed to predict the uptake rate of the adsorbate onto the adsorbent. Pseudo-first-order (PFO) [Lagergren, 1898] and pseudo-second-order (PSO) [Blanchard et al., 1984] models are the two most commonly used empirical models in liquid adsorption studies. As empirical models, PFO and PSO can adequately describe experimental data of adsorption kinetics, however, fail to explain the adsorption mechanisms. Some diffusion models were developed based on the rate limiting step during adsorption process. Such as intra-particle diffusion (IPD) model [Weber and Morris, 1963], Boyd's external diffusion model [Boyd et al., 1947] and Frusawa and Smith (F&S) model [Furusawa and Smith, 1973].

Multiple mathematical models have been used to describe and predict the breakthrough curves of a column adsorption system. Abu-Lail et al. [2012] measured the

adsorption breakthrough curve of chloroform on MFI zeolite granules in fixed-bed columns, and predicted the breakthrough curves using the film-pore and surface diffusion (FPSD) model. In the research done by Heijman et al. [2002], the combination of mass transfer model and Freundlich isotherm model was used to predict the breakthrough curve of atrazine in a column packed with GAC. Han et al. [2008] carried out a research on the continuous fixed bed by using rice husk as a biosorbent for the removal of congo red from aqueous solution where Thomas, Adams–Bohart, and Yoon–Nelson models were applied to experimental data to predict the breakthrough curves.

1.5 KNOWLEDGE GAPS AND RESEARCH OBJECTIVES

According to the literature, there are several knowledge gaps to be further investigated. First of all, OMP adsorption by zeolite powders has been well studied in batch mode, however, the performance of zeolite granules and the application in packed columns was seldom investigated. Secondly, the WW effects on the performance of zeolite granules were unknown. Third, for the pilot and full-scale application of zeolite granules, a comprehensive model will be useful to predict the breakthrough of OMPs and help optimize operation parameters, which deserves more attention.

According to the research background and the stated knowledge gaps, the major objectives in this research were:

1. To promote better understanding of the adsorption capacity and kinetics of the 11 target OMPs by zeolite granules.

2. To understand the effects of WW on the performance of zeolite granules.

3. To establish a mathematical model to predict OMP breakthrough curves of zeolite-granule packed column under different operating conditions.

1.6 RESEARCH QUESTIONS AND APPROACHES

To meet the research objectives, the following research questions are formulated:

1. What are the adsorption capacity and kinetics of 11 OMPs by zeolite granules in demineralised water (demi-water)?

2. What are the effects of WW on the performance of zeolite granules?

3. What are the OMP breakthrough curves of zeolite-granule packed column under different empty bed contact times (EBCTs)?

4. Can we predict the breakthrough curves using a mathematical model with the isotherm and kinetic constants from batch experiments?

To answer the research questions, the research approaches can be divided into four steps as shown in Figure 1.1:

Step I: Determined the adsorption isotherms of 11 OMPs by zeolite powders in demi-water and WW in batch experiment.

Step II: Determined the adsorption kinetics of 11 OMPs by zeolite granules in demi-water and WW in batch experiment.

Step III: Found out the breakthrough curves of 11 OMPs in zeolite-granule packed columns under different EBCTs. Due to the Coronavirus outbreak event in January 2020, WW was not available for research. Therefore, only demi-water solution was used in the column experiments.

Step IV: Established a mathematical model to predict the OMP breakthrough curves in the columns. Evaluated the model by comparing the modelled results with the experimental results.
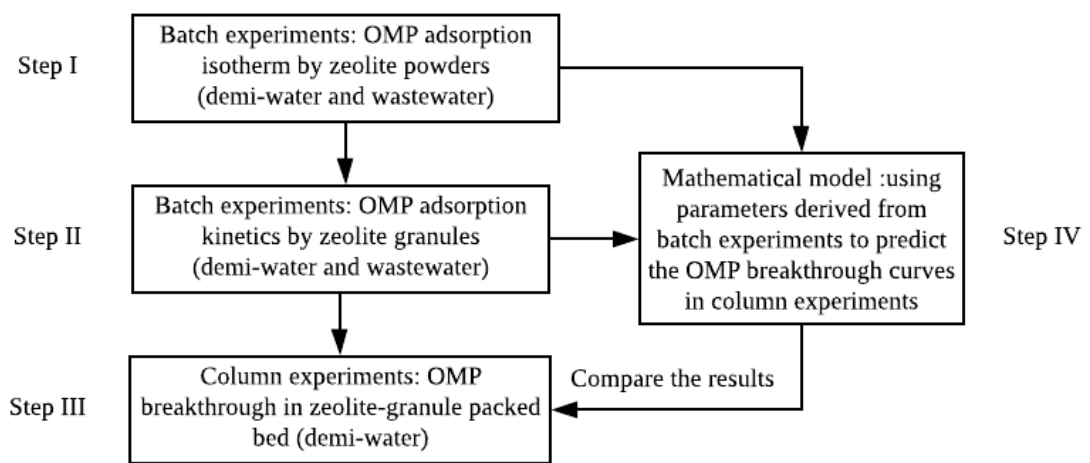
Figure 1.1: Flowchart of general experiment design

2 | MATERIALS AND METHODS

2.1 MATERIALS

2.1.1 Zeolites

According to the research done by [Jiang, 2019], among the four mentioned framework types of zeolite in Table 1.1, BEA and MOR types were of better performance on the adsorption of several OMPs, because the pore openings of BEA and MOR are large enough to allow certain OMPs to enter, and BOMs with larger sizes will be excluded from adsorption. Therefore, BEA and MOR zeolites were studied in this research. Both of them were provided by Tosoh Corporation. The characteristics of zeolites are listed in Table 2.1.

Table 2.1: Names and characteristics of high-silica zeolite powders

Zeolite type	Product name	Cation[a]	Pore size[a] (Å)	Si/Al[a]	Surface area[a] (m²g⁻¹)	Particle size[a] (µm)
BEA	HSZ-980HOA	H⁺	6.5	500	250	2.5
MOR	HSZ-690HOA	H⁺	7	240	120	12

[a] All the listed characteristics are provided by the supplier.
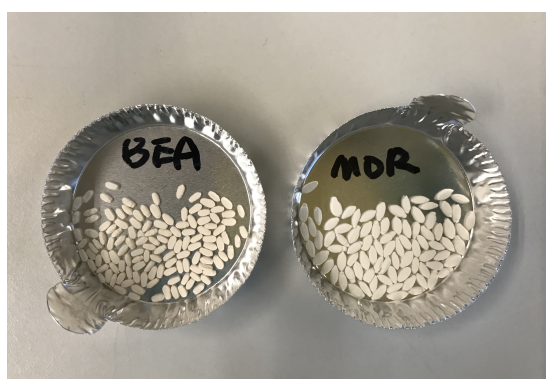
(a) Zeolite granules

(b) 3D printing

Figure 2.1: Preparation of zeolite granules

Zeolite granules applied in this research were prepared by mixing zeolite powders with bentonite (Sigma-Aldrich). The weight ratio of zeolite/bentonite is 85/15. After adding adequate amount of demi water to reach certain viscosity, the mixture of zeolite powder and bentonite was made into granules with uniform rice-like shape by 3D printer. The printed granules were sintered under 950 °C for 2 hours.

Due to different properties of the two zeolite powders, the printed granules of BEA and MOR were of different sizes. BEA granule had a thickness of 1 mm, a width of 2 mm, and a length of 3mm. MOR granule had a larger size, with a thickness of 1 mm, a width of 2 mm, and a length of 3.5 mm (as shown in Figure 2.1). The granule density was 1.18 g/mL for BEA granules and 0.71 g/mL for MOR granules.

2.1.2 OMPs

The physicochemical properties of the 11 target OMPs can be found in Table 2.2. The chemical structures of the OMPs are listed in Appendix A.

Table 2.2: Physicochemical property of OMPs [*]

Name [a]	log D at pH6.5 [b]	MW (g/mol)	Strongest acidic pKa [b]	Strongest basic pKa [b]	Charge at pH6.5 [b]	Minimum projection radius (Å) [b]	Maximum projection radius(Å) [b]
Carbamazepine (Carba.)	2.77	236.27	15.96	-	0	4.48	5.7
Hydrochlorthiazide (Hydro.)	-0.58	297.74	9.09	-	0	4.13	5.67
Propanolol (Propra.)	-0.32	259.34	14.09	9.67	+	4.66	7.41
Metoprolol (Metop.)	-1.14	267.36	14.09	9.67	+	4.39	10.07
Sotalol (Sotalol.)	-2.82	272.36	10.07	9.43	+	4.21	7.94
Trimethoprim (Trime.)	0.60	290.32	-	7.16	+	4.97	6.95
Clarithromycine (Clari.)	0.78	747.95	12.46	9	+	7.7	8.47
1H-Benzotriazol (Benzo.)	1.3	119.12	9.04	0.22	-	3.66	4.12
Methyl-benzotriazol (Methyl-benzo.)	1.81	133.15	9.12	0.45	-	4.05	4.43
Sulfamethoxazole (Sulfa.)	0.38	253.28	6.16	1.97	-	5.4	5.88
Diclofenac (Diclo.)	1.79	296.15	4	-	-	-	-

[a] Abbreviations will be used in the tables and figures in the following discussion.
[b] Estimated by Chemicalize Platform.
[*] The OMPs are sorted by charge, and an ascending trend in molecular weight.

2.1.3 Water

Demi-water and WW were used to prepare the solutions. The pH of demi-water was in the range of 5.3-6.2. The WW was collected from Horstermeer, Waternet and was not available for research since January 2020 due to the Coronavirus outbreak event. The characteristics of the collected WW are shown in Table 2.3.

Table 2.3: Characteristics of WW

	Value	Unit
COD	20.9	mg/L
PO_4^--P	0.18	mg/L
Total nitrogen	4.9	mg/L
SO_4^{2-}	30.2	mg/L
pH	8.0-8.2	-
EC	426.9	µs/cm
DO	9.3	mg/L
DOC	6.7-7.4	mg/L

2.2 EXPERIMENTS

2.2.1 Stock solution preparation

The stock solution was prepared by dosing 2 mg of each OMP in 10 L ultrapure water (ELGA, Ultra AN MK2 ultrapure water system) to obtain the concentration of approximately 0.2 mg/L. The stock solution was kept in the refrigerator under 4 °C.

2.2.2 Adsorption isotherms

Batch experiments in demi-water and WW were conducted to obtain the adsorption isotherms of 11 OMPs by BEA and MOR zeolite. To shorten the experiment time, zeolite powders were used in the isotherm test to represent the adsorption capacity of OMPs by zeolite granules. The flowchart of the experiments can be found in Figure 2.2. The solution for experiments was prepared by spiking stock solution in demi-water and WW to obtain OMP concentrations of $\sim$ 4 µg/L. The pH of the 4 µg/L demi-water solution was in the range of 5.4-6.5 (with the addition of zeolite, an increase of pH was observed). The pH of the 4 µg/L WW solution was in the range of 8.0-8.3.

Different weight of zeolite powders (0, 1, 5, 10, 50, 100, 250, 500 and 1000 mg) were dosed in Duran glass bottles with 1 L solution. The solution with zeolite dosage of 0 mg was used as blank to test the stability of the OMPs over the whole testing time. The sampling times for demi-water experiments were 24h and 48h, however, longer equilibrium time was expected in WW experiments, therefore the sampling times of 1d and 8d were designed in WW experiments. Water samples were taken and filtrated by 0.2 µm syringe filter (Regenerated Cellulose, Spartan, Whatman) prior to the analysis of Liquid chromatography combined with tandem mass spectrometry (LC-MS).

(a) Demi-water   (b) Wastewater
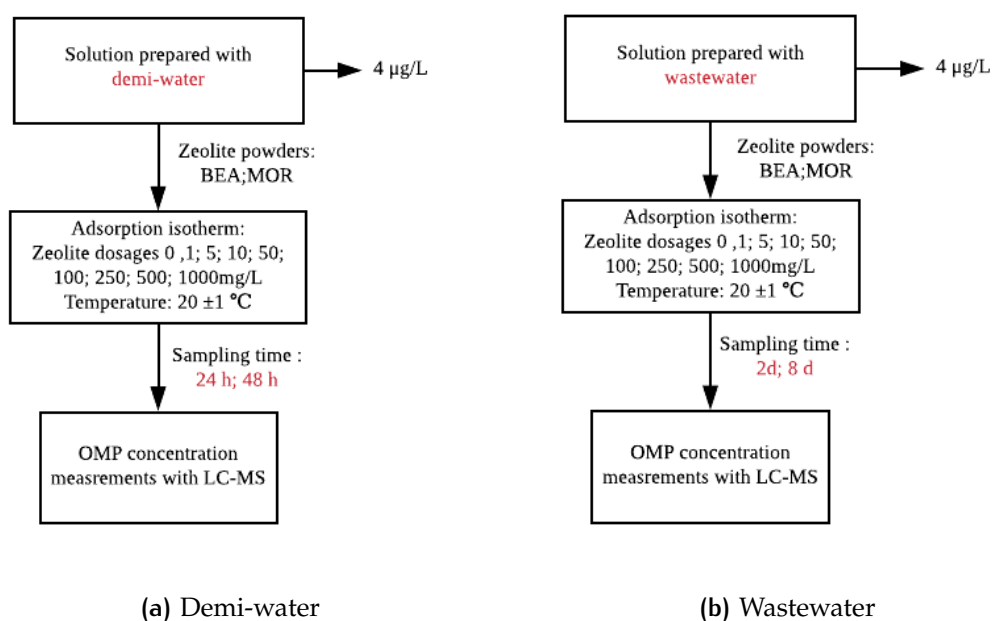
Figure 2.2: Flowchart of isotherm experiments

2.2.3 Adsorption kinetics

The batch experiments of adsorption kinetics were carried out using BEA and MOR granules in demi-water; while due to the limited WW storage, only BEA granules were used to study the effect of WW on kinetics. The flowchart can be found in Figure 2.3.

The solution for kinetics experiment was prepared by spiking stock solution in demi-water and WW to obtain OMP concentrations of $\sim$4 µg/L. Zeolite granules with the weight of 0, 50, 250 and 500 mg were dosed in 1L solution in Duran glass bottles. The solution with zeolite dosage of 0 mg/L was used as blank to test the stability of the OMPs over the whole testing time. The operating time was 25 days. Approximate 1 mL sample was collected at different time points. Samples were filtrated by 0.2 µm syringe filter before LC-MS analysis.

(a) Demi-water   (b) Wastewater
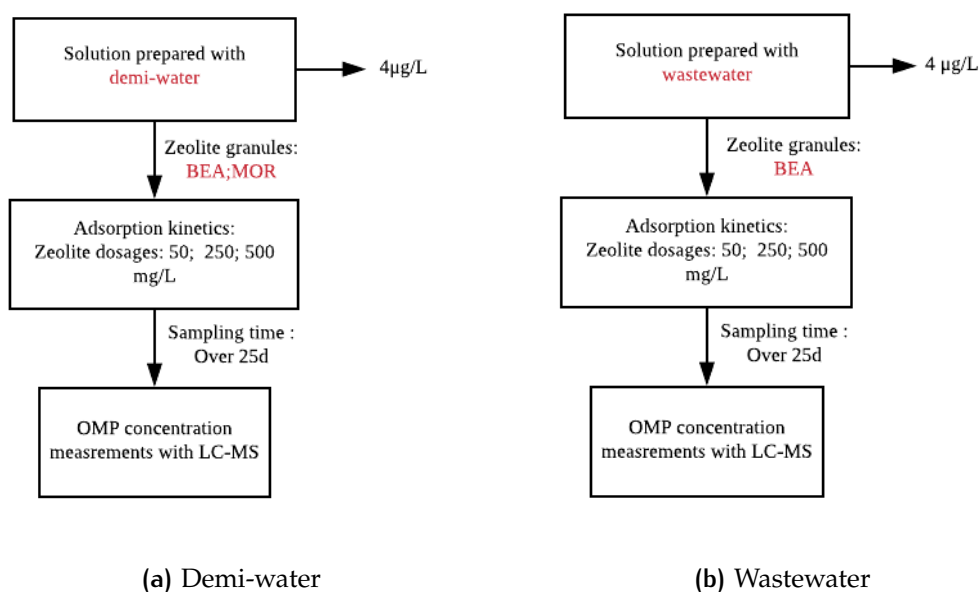
Figure 2.3: Flowchart of kinetics experiments

2.2.4 Column experiments

The breakthrough curves of 11 OMPs were obtained by running the columns packed with zeolite granules. Due to limited WW storage in the later stages of the research, only demi-water solution was used in the column experiments. The flowchart of the experiments can be found in Figure 2.4. The operating parameters of the column experiments are listed in Table 2.4.

The inner diameter of the column was 1.89 cm and the total length of the column was 40 cm. The packed height of zeolite granules were set equal in all columns as 10 cm, the empty bed contact times (EBCTs) were set as 6 minuets and 20 minuets, by varying the flow velocity one can obtain different EBCTs. The solution for column experiments was prepared by spiking stock solution in demi-water to obtain OMP concentrations of $\sim$ 4 μg/L. The solution was transported to the vertical column from the top with the feed flow rates of 4.68 mL/min and 1.4 mL/min, respectively. After packing the granules, the porosity of the column can be measured by filling the column with water then draining the column, and measuring the volume of water in the pores.

The column experiments were operated for 14 days and the outlet flow samples were collected using auto-samplers. The sampling time interval was 3 hours. After filtration, the samples were analyzed by LC-MS to obtain OMP concentrations.

(a) EBCT of 6 min

(b) EBCT of 20 min
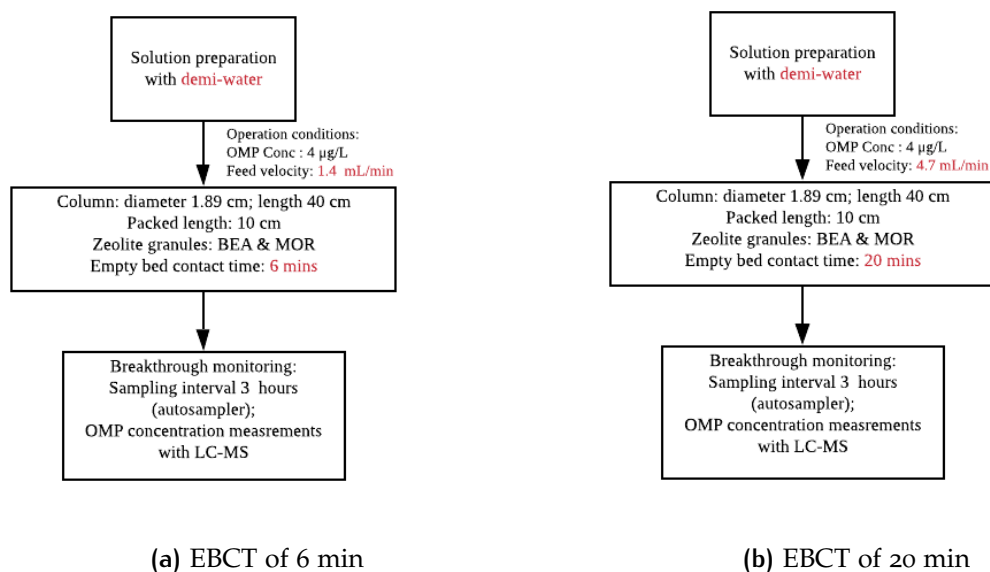
Figure 2.4: Flowchart of column experiments

Table 2.4: Column experiment operating parameters

	MOR		BEA		
	Column A	Column B	Column A	Column B	Unit
Column diameter	1.89	1.89	1.89	1.89	cm
Packed Volumn	28.06	28.06	28.06	28.06	ml
Bulk density	0.40	0.40	0.72	0.72	g/ml
Particle density	0.71	0.71	1.18	1.18	g/ml
Porosity	0.43	0.43	0.39	0.39	-
Packed length	10.00	10.00	10.00	10.00	cm
Packed weight	10.14	10.14	20.09	20.09	g
EBCT	20.00	6.00	20.00	6.00	min
Flow rate	1.40	4.68	1.40	4.68	ml/min
Superficial velocity	0.50	1.67	0.50	1.67	cm/min

2.2.5 Analysis

Methods

High performance liquid chromatography combined with tandem mass spectrometry (LC-MS) were used to quantify OMPs. Gradient elution using ultrapure water and acetonitrile (LC-MS grade, Biosolve, France) phases, both acidified with 0.1 % LC-MS grade formic acid (Biosolve, France), was applied on an ACQUITY UPLC®

BEH C18 (1.7µm particle size, 2.1x50 mm, Waters, Ireland) column, at a flow rate of 0.35 ml/min, pumped by an ACQUITY UPLC I-Class Plus (Waters, USA). Tandem mass spectrometry was conducted on a Xevo TQ-S micro (Waters, USA), equipped with electrospray ionization in positive and negative modes, detecting two daughter ions from mother ion of each OMP compound and corresponding deuterated internal standards, with quantification by the calibration at levels from 0.0025 µg/L to 10 µg/L. Data were evaluated with TargetLynx software. The preparation of standards is shown in Appendix F, MS parameters and quantification ions are shown in Appendix H.

Problems with concentration measurement

The concentration of OMPs at µg/L level were measured with LC-MS. However, there are some problems associated with the measurements of propranolol, clarithromycin and hydrochlorothiazide.

Before the LC-MS measurement, samples needed to be filtered through 0.2 µm filters to remove particles. It can be noticed that the data of propranolol was always below the detecting limit in the demi-water even at $\sim$ 4 µg/L. However, the concentration of propranolol can be well measured in WW. The reason might be that propranolol in demi-water was absorbed by the 0.2 µm filters before measuring the concentrations in LC-MS. In WW, the adsorption sites of the filters were first occupied by BOMs since the concentration of BOMs (several mg/L) was much higher than the concentration of OMPs (a few µg/L). Thus, the concentration of propranolol was not affected that much. Clarithromycin cannot be well measured by LC-MS, which might be due to the large molecular size of this compound. In addition, hydrochlorothiazide was analyzed in negative electrospray ionization (ESI-) mode. Compared with OMPs measured in ESI+ mode, LC-MS had higher detection limit and lower accuracy for the measurement of hydrochlorothiazide. Except for propranolol, clarithromycin and hydrochlorothiazide, the measurement for the other OMPs were of high accuracy.

2.3 ADSORPTION ISOTHERM AND KINETICS MODELS

2.3.1 Freundlich isotherm

Freundlich isotherm is frequently used to describe the adsorption of OMPs with low concentration in water, e.g. the range of ng/L and µg/L [Xu et al., 2013]. As the concentration of OMPs in this study was in a low range, the maximum adsorption capacity of zeolite would not be reached, thus, the Freundlich isotherm was used to

fit the isotherm data. The nonlinear and log-log transformation forms of Freundlich equation are shown in Equation 2.1 and Equation 2.2:

$$q_e = K_F C_e^n \tag{2.1}$$

$$\log q_e = n \log C_e + \log K_F \tag{2.2}$$

where q_e (µg/mg) is the equilibrium adsorption amount, C_e (µg/L) is the equilibrium concentration, K_F (µg/mg)/(µg/L)^n is the Freundlich constant, and n (dimensionless) is the Freundlich intensity parameter.

2.3.2 Linear isotherm

The linear isotherm is a special case of Freundlich isotherm where the Freundlich intensity parameter n is equal to 1. The equation is expressed as Equation 2.3.

$$q_e = K_L C_e \tag{2.3}$$

where q_e (µg/mg) is the equilibrium adsorption amount, C_e (µg/L) is the equilibrium concentration, and K_L is the linear isotherm constant (L/mg). This isotherm model describes a suitable fit for the adsorption of adsorbate at relatively low concentrations, where all adsorbate molecules are secluded from their nearest neighbors [Helfferich, 1984].

2.3.3 Pseudo first order kinetics

In order to reduce the computational complexity involved in breakthrough modelling (described later), PFO model Lagergren [1898] was used to fit the kinetic data. The equation of PFO model is shown below Equation 2.4. Integrating Equation 2.4 for the condition of $q_o = 0$ yields Equation 2.5.

$$\frac{dq_t}{dt} = k_{PFO}(q_e - q_t) \tag{2.4}$$

$$q_t = q_e \left(1 - e^{-k_{PFO}t}\right) \tag{2.5}$$

where q_e and q_t are the adsorption amounts (µg/mg) at equilibrium and at any time t (h), respectively; k_{PFO} (1/h) is the rate constant of the PFO equation.

The *Curve _ fit()* function in Python with nonlinear least squares was used to find the optimal parameter that gave the smallest error. There were two methods to determine the equilibrium loading (q_e) in the PFO kinetics model. Firstly, q_e was estimated by OMP adsorption isotherms by powder zeolites using Equation 2.6. With known C_0, W and Freundlich constants (K_F and n), the only unknown value is C_e, and q_e can be further calculated from the obtained C_e. Secondly, except for the theoretical q_e obtained with OMP adsorption isotherms by powder zeolites, q_e can also be obtained by the curve fitting process, which was recognized as the plateau of the kinetic curve.

$$\frac{(C_0 - C_e)\,V}{W} = K_F C_e^n \tag{2.6}$$

where C_0 (µg/L) is the initial concentration, C_e (µg/L) is the equilibrium concentration, V (L) is the volume of the solution, W (mg/L) is the zeolite dosage, K_F (µg/mg)/(µg/L)^n and n are the Freundlich constants.

2.3.4 Intra-particle diffusion kinetics

The linearized transformation of the IPD model [Weber and Morris, 1963] is presented as following:

$$q_t = k_p \sqrt{t} + C \tag{2.7}$$

where k_p (µg/(mg × h$^{1/2}$)) is the rate constant of the IPD model and C (µg/mg) is a constant associated with the thickness of the boundary layer, where a bigger value of C means a greater limiting effect on the boundary layer. If a plot of q_t against $t^{0.5}$ is linear and passes through the axis origin, the adsorption is entirely governed by intra-particle diffusion. Conversely, if the intra-particle diffusion fit gives multiple linear regions, the adsorption process is controlled by a multi-step mechanism [Tran et al., 2017].

2.3.5 Error analysis

The effectiveness of the fitting was evaluated by the coefficient of determination (R^2 Equation 2.8).

$$R^2 = 1 - \frac{\sum \left(q_{\text{exp}} - q_{cal}\right)^2}{\sum \left(q_{\text{exp}} - q_{\text{mean}}\right)^2} \tag{2.8}$$

where q_{exp} (µg/mg) is the amount of adsorbate uptake obtained from experiments, q_{cal} (µg/mg) is the amount of adsorbate uptake estimated by the model, and q_{mean} (µg/mg) is the mean of the q_{exp} values.

2.4 BREAKTHROUGH MODEL

2.4.1 One-dimensional mass transfer model

One-dimensional mass transfer model was applied to predict OMP breakthrough curves in column experiments. The concentration of the adsorbents varies with the function of time and position in the column. The concept is shown in Figure 2.5. OMP concentration in the outflow of the column was influenced by:

- convective mass transfer;

- axial dispersion;

- adsorbed by adsorbent.

1:convective mass transfer
2:axial dispersion
3:adsorbed by adsorbent
4:concentration change

$(1+)-(1-): -v\frac{\partial c}{\partial z}$

$(2+)-(2-): -D_L\frac{\partial^2 c}{\partial z^2}$

$(3-): -[\frac{1-\varepsilon}{\varepsilon}]\rho\frac{\partial q}{\partial t}$

$(4): \frac{\partial c}{\partial t}$
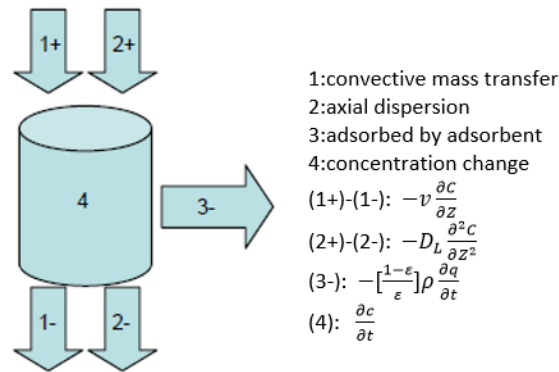
Figure 2.5: Schematic diagram of the mass conservation of a control volume (cited from Xu et al. [2013])

A macroscopic mass conservation equation was acquired to represent the relationship between the above mentioned terms:

$$\frac{\partial c}{\partial t} = D_L\frac{\partial^2 c}{\partial z^2} - v\frac{\partial c}{\partial z} - \left[\frac{1-\varepsilon}{\varepsilon}\right]\rho_b\frac{\partial q}{\partial t} \tag{2.9}$$

The PFO kinetic equation Equation 2.4 and Freundlich equation Equation 2.1 were substituted into the partial differential equation (in the term $\frac{\partial q}{\partial t}$). In which,

- c is the concentration of a certain species;

- D_L is the dispersion coefficient;

- v is the superficial velocity of the water phase in the packed bed;

- ε is the porosity of the packed bed;

- ρ_b is the bulk density of the zeolite granules;

- q is (amount of adsorbate adsorbed)/(amount of adsorbent used for adsorption).

The assumptions made to this model include [Xu et al., 2013]:

- the process is isothermal;

- no chemical reaction occurs in the column;

- the packing material is spherical and uniform in size;

- the bed is homogeneous and the concentration gradient in the radial direction of the bed is negligible;

- the flow rate is constant and invariant with the column position.

The dispersion coefficient (D_L) was determined by feeding the column with NaCl solution and measuring the conductivity of the outflow over time. As the adsorption of NaCl by zeolites was negligible, Equation 2.9 was simplified to a differential equation with only the dispersion and the convection terms in the packed bed. By fitting the breakthrough curve of NaCl, D_L can be calculated.

With the adsorption isotherm and kinetic parameters from batch experiments, the D_L from the NaCl method, and the process parameters of the columns (OMPs initial concentrations, superficial velocity, particle density, porosity, column packed height and column intersection area), the OMP concentration change over time can be calculated. COMSOL Multiphysics 5.4 was used to compute the partial differential equation. The computed results were compared to the tested results to verify the correctness of the model, and to evaluate the feasibility of the model for the scale-up predicting.

2.4.2 COMSOL implementation

The dimensionless forms of Equation 2.1, Equation 2.4 and Equation 2.9 used in the COMSOL modelling were displayed below.

The dimensionless overall mass balance equation:

$$-\frac{1}{Pe}\frac{\partial^2 x}{\partial l^2} + \frac{\partial x}{\partial l} + \frac{\partial x}{\partial \tau} + D_g\frac{\partial y}{\partial \tau} = 0 \tag{2.10}$$

The dimensionless kinetics equation:

$$\frac{\partial y}{\partial \tau} = S\left(y^* - y\right) \tag{2.11}$$

The dimensionless isotherm equation:

$$y^* = \frac{K_F \cdot (C_0 \cdot x)^n}{q_0^*} \tag{2.12}$$

The symbol * represents equilibrium state. The definition and expression of all the dimensionless variables appeared in the equations can be found in Table 2.5.

Table 2.5: Dimensionless variables used for Comsol implementation

Variable	Expression
Concentration of OMPs in liquid phase [a]	$x = \frac{c}{c_0}$
Concentration of OMPs in solid phase [b]	$y = \frac{q}{q_0^*}$
Distance from the bed entrance	$l = \frac{z}{L}$
Time	$\tau = \frac{t \cdot v}{L}$
Distribution coefficient	$D_g = \frac{\rho_b \cdot q_0^*}{\varepsilon \cdot C_0}$
Mass transfer coefficient	$S = \frac{K_G \cdot L}{v}$
Peclet number	$Pe = \frac{L \cdot v}{D_z}$

The dimensional variables are shown below:

- C_0 is the OMP initial concentration (µg/L);

- q_0^* is the adsorption loading in equilibrium with the initial concentration (µg/mg) ($q_0^* = K_F \cdot C_0^n$);

- z is the distance from the bed entrance (m);

- L is total bed depth (m);

- v is the superficial velocity of the water phase in the packed bed (m/s);

- ρ_b is the bulk density of the packed zeolite granules (kg/m³).

- ε is the porosity of the packed bed;

- K_G is kinetic constant (1/s);

- K_F is the Freundlich isotherem constant (µg/mg)/(µg/L)ⁿ;

- n is the exponent in the Freundlich isotherm (-);

- D_z is the dispersion coefficient (m²/s).

The model was implemented with a **time-dependent & one-dimensional coefficient form partial differential equations module (coefficient form PDE)**. The partial differential equation was solved numerically with the finite element method, using the vector variable u ($\begin{bmatrix} x \\ y \end{bmatrix}$) :

$$e_a \frac{\partial^2 u}{\partial t^2} + d_a \frac{\partial u}{\partial t} + \nabla(-c\nabla u - \alpha u + \gamma) + \beta \nabla u + au = f \tag{2.13}$$

By defining the coefficient (2-by-2 matrices or 2-by-1 vectors) in the template, one can match the partial differential equation that we have (Equation 2.10) to the template. The coefficient matrices (or vectors) were defined as following:

$$e_a = \begin{bmatrix} 0 & 0 \\ 0 & 0 \end{bmatrix} \quad d_a = \begin{bmatrix} 1 & D_g \\ 0 & 1 \end{bmatrix} \quad c = \begin{bmatrix} 1/\text{Pe} & 0 \\ 0 & 0 \end{bmatrix} \quad \alpha = \begin{bmatrix} -1 & 0 \\ 0 & 0 \end{bmatrix} \quad \gamma = \begin{bmatrix} 0 \\ 0 \end{bmatrix}$$

$$\beta = \begin{bmatrix} 0 & 0 \\ 0 & 0 \end{bmatrix} \quad a = \begin{bmatrix} 0 & 0 \\ 0 & S \end{bmatrix} \quad f_{\text{Freu}} = \begin{bmatrix} 0 \\ \frac{SK_F(C_0 x)^n}{q_0^*} \end{bmatrix}$$

In the initial state, the OMP concentrations in both liquid and solid phase were zero. At the top boundary, the dimensionless concentration x equaled 1, which was a Dirichlet boundary condition. At the bottom boundary, the change of concentration along the length was zero, which was a Neumann boundary condition. The initial condition and boundary conditions were formulated as:

$$\tau = 0: \quad x = 0, y = 0 \quad (0 \leqslant l \leqslant 1)$$
$$l = 0: \quad x = 1 \quad (\tau > 0)$$
$$l = 1: \quad \frac{\partial x}{\partial l} = 0 \quad (\tau > 0)$$

2.4.3 Sensitivity analysis

Through sensitivity analysis, the influence of the most important parameters on breakthrough curve modelling was investigated, including D_L, granule bulk density, porosity, packing height and flow velocity. The sensitivities of the model to these parameters were check by changing the parameters by ±30%, and comparing with the base case.

3 | RESULTS AND DISCUSSION

3.1 ADSORPTION ISOTHERMS OF OMPS BY ZEOLITE POW–DERS

The experiments of OMP adsorption isotherms by BEA and MOR zeolite powder were designed with eight zeolite dosages: 1, 5, 10, 50, 100, 250, 500 and 1000 mg/L. However, the OMP removal at zeolite dosage of 1 mg/L and 5 mg/L was minimal, hence, the data points at these two dosages were removed from the plotting and fittings. In this section, the fittings of Freundlich isotherm on the data and the factors that affect the adsorption capacities will be elaborated, including OMP characteristics, zeolite characteristics and WW matrix.

3.1.1 Adsorption capacity overview and Freundlich isotherm fittings

According to the removal percentage of OMPs at zeolite dosage $\geqslant$ 50 mg/L, 11 OMPs can be divided into three categories: good removal ($>$ 95%), medium removal (20% – 95%) and bad removal ($<$ 20%). The overview of the adsorption capacity of the 11 OMPs are listed in Table 3.1. The removal percentages at zeolite dosage of 50 mg/L are presented in brackets.

By looking at the demi-water results presented in Table 3.1, BEA and MOR zeolites had high removal capacities for trimethoprim, propranolol, metoprolol, sotalol and clarithromycin; had medium-removal for 1H-benzotriazole, methyl-benzotriazole and sulfamethoxazole; and had bad-removal for Diclofenac. What should be noticed is that carbamazepine belonged to the category of "bad removal" in the BEA case, however, belonged to the category of "medium removal" in the MOR case.

Table 3.1: Adsorption capacity overview of OMPs in demi-water and WW by BEA and MOR zeolite powders

Name	BEA Demi	BEA WW	MOR Demi	MOR WW
Trime.	Good (99%)	Medium (88%)	Good (99%)	Bad (15%)
Propra.[a]	Good (99%)	Medium (93%)	Good (99%)	Good (99%)
Metop.	Good (98%)	Medium (92%)	Good (99%)	Good (99%)
Satolol.	Good (99%)	Medium (88%)	Good (99%)	Good (99%)
Clari.[a]	Good (99%)	Bad (1%)	Good (98%)	Bad (13%)
Benzo.	Medium (24%)	Bad (2%)	Medium (50%)	Bad (2%)
Methyl-benzo.	Medium (71%)	Medium (56%)	Medium (87%)	Medium (55%)
Hydro.[a]	Medium (26%)	Medium (62%)	Medium (22%)	Bad (15%)
Sulfa.	Medium (41%)	Bad (6%)	Medium (51%)	Bad (2%)
Carba.	Bad (5%)	Bad (4%)	Medium (47%)	Bad (8%)
Diclo.	Bad (6%)	Bad (1%)	Bad (9%)	Bad (6%)

[a] The data for hydrochlorothiazide, clarithromycin in demi-water and WW, and the data for propranolol in demi-water were of relatively low accuracy, however, the capacity categories of these three OMPs should be correct.

The dose-response relation identified in the data is the prerequisite for plotting the isotherm. The equilibrium concentration of the well adsorbed compounds were close to zero at all dosages, and thus, the dose-response relations can hardly be identified. Similarly, the equilibrium concentration of compounds with poor removal capacity were high and close to the initial concentration, resulting in inaccurate calculation of adsorption capacity. Thus, in demi-water, the adsorption isotherms of OMPs with medium removal capacity are presented in Figure 3.1. The Freundlich isotherm fitting constants are shown in Table 3.2.
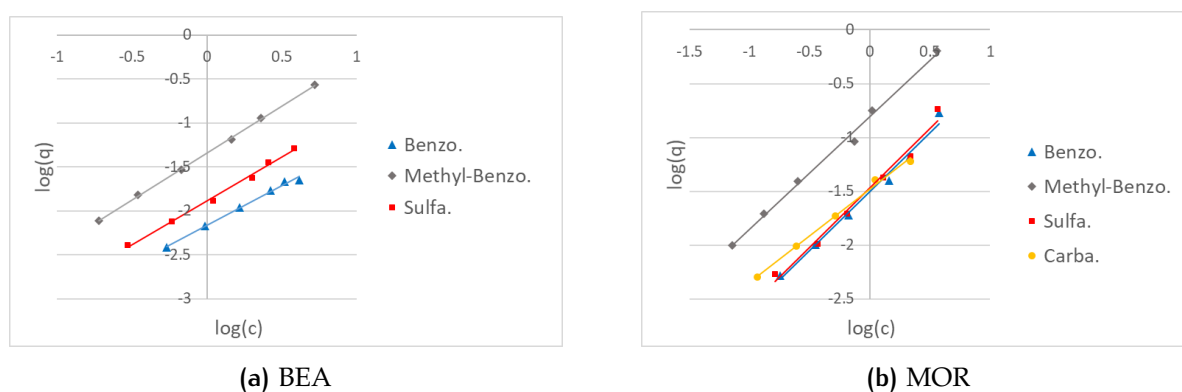

(a) BEA   **(b)** MOR

Figure 3.1: Log-Log Freundlich isotherm fitting of medium-removal OMPs in demi-water by BEA and MOR zeolite powders

Table 3.2: Freundlich fitting constants for OMP adsorption in demi-water by BEA and MOR zeolite powders

	BEA			MOR			
	Benzo.	Methyl-benzo.	Sulfa.	Benzo.	Methyl-benzo.	Carba.	Sulfa.
K_F[a]	0.0069	0.0457	0.0129	0.0204	0.1177	0.0207	0.0224
n	0.8965	1.0691	0.9941	0.9017	1.0142	0.6836	0.9325
R^2	0.9932	0.9994	0.9948	0.9961	0.9948	0.9384	0.9969

[a] Unit: $(\mu g/mg)/(\mu g/L)^n$

As reported by Giles et al. [1974], adsorption isotherms can be divided into the four groups (Figure 3.2). The C-shaped adsorption isotherm describes the linear increase of OMP adsorption loading with the OMP equilibrium concentration in water, which means the adsorbed molecules were secluded from their nearest neighbors [Helfferich, 1984]. The C-shaped isotherm was typically observed under low OMP concentrations (ng/L- µg/L) [Limousin et al., 2007]. In the L-shaped and H-shaped isotherms, plateaus can be observed at high equilibrium concentrations, which means that the adsorbent with limited adsorption sites has reached a saturated state. The S-shaped isotherm indicates the lack of adsorption affinity for OMPs at low equilibrium concentration [Jiang et al., 2020].
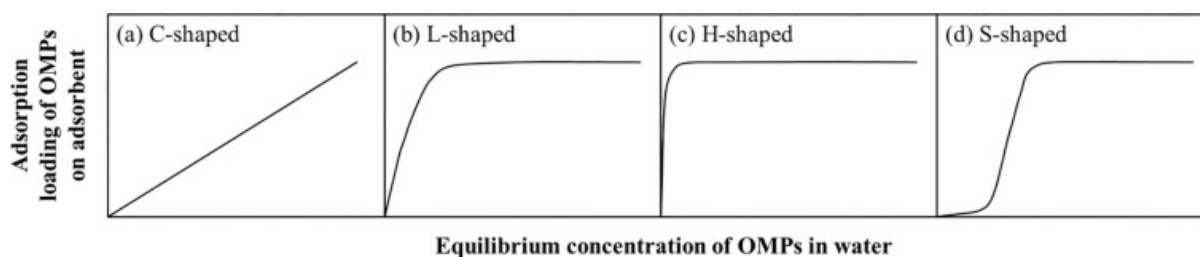

Figure 3.2: The four characteristic types of adsorption isotherms [Giles et al., 1974]

From Table 3.2, the n value for 1H-benzotriazole, methyl-benzotriazole and sulfamethoxazole were all close to 1, giving C- shaped isotherms. However, the n value from carbamazepine adsorption by MOR zeolite was 0.68, indicating a bend curve of the isotherm. The isotherm of carbamazepine by BEA and MOR are plotted in the original scale (without log-log transformation) and shown in Figure 3.3. In the case of BEA, the isotherm was likely the initial stage of a S-shaped curve. In the case of MOR, the isotherm was possibly L-shaped.
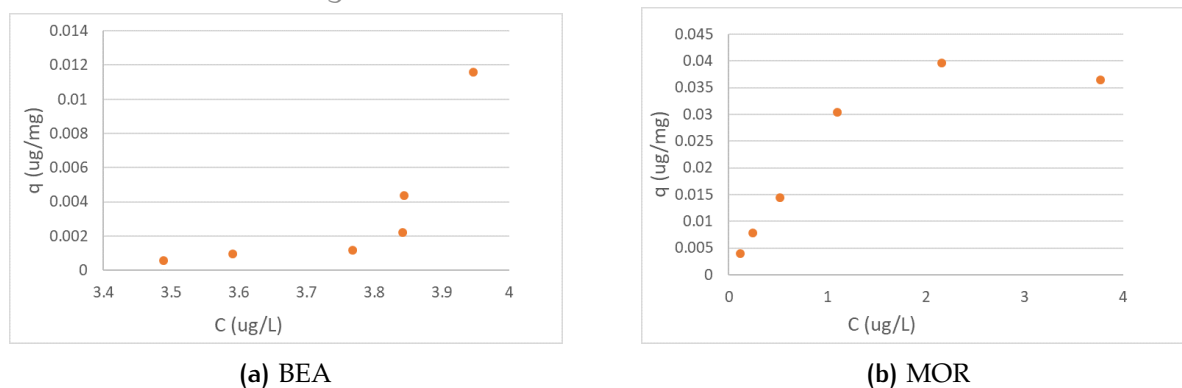
(a) BEA

(b) MOR

Figure 3.3: Adsorption isotherms of carbamazepine in demi-water by BEA and MOR zeolite powders

3.1.2 Effect of OMP characteristics

Charge of OMPs

By referring to OMP characteristics in Table 2.2, one can see that the five well adsorbed OMPs (trimethoprim, propranolol, metoprolol, sotalol and clarithromycin) were all positively charged at pH 6.5 (pH of the demi-water solution). However, OMPs with lower adsorption capacity were either negatively or neutral at pH 6.5. Therefore, it can be inferred that the electrostatic attraction between positively charged OMPs and the negatively charged sites on the zeolite surface is the main mechanism that affects the adsorption capacity of zeolites for OMPs. The charge effect on OMP adsorption by zeolites was also observed by [Jiang, 2019], finding that positively charged pharmaceuticals were better adsorbed on zeolites than negative and neutral charged pharmaceuticals.

Size of OMPs

When the maximum dimension of the long-chain molecule was larger than the pore opening of the zeolite, this molecule would hardly enter the pores on zeolite. According to the chemical structure of OMPs listed in Appendix A, it can be found that, the good-removal OMPs (trimethoprim, propranolol, metoprolol, sotalol and clarithromycin) all have long-chain structures compared with other OMPs. Besides, no special relation between the size of the OMPs (Table 2.2) and size of the zeolite pores (Table 1.1) was found. It was also found that the minimum projected diameters (twice the radius) estimated by Chemicalize Platform of all the 11 OMP are greater than the pore size of the BEA and MOR zeolite. Therefore, it can be concluded that the size of OMPs should not be the main factor affecting the adsorption capacity, and OMPs were preferably adsorbed on the external surface of zeolites instead of entering the pores.

Hydrophobicity of OMPs

From the isotherm fitting displayed in Figure 3.1, the adsorption capacity of OMPs follow the order of methyl-benzotriazole >sulfamethoxazole >1H-benzotriazole. Carbamazepine was poorly removed by BEA thus the isotherm cannot be plotted. However, the adsorption capacity of carbamazepine by MOR was relatively high and close to that of sulfamethoxazole and 1H-benzotriazole.

It can be noticed that methyl-benzotriazole and 1H-benzotriazole had similar chemical structure, while methyl-benzotriazole had higher adsorption capacity. By looking at the chemical structure of OMPs in Appendix A, the only difference between 1H-benzotriazole and methyl-benzotriazole is that the latter one has a methyl functional group attached on the aromatic ring. Notably, sulfamethoxazole that had higher adsorption capacity than 1H-benzotriazole also has a methyl functional group in the structure. According to Leung et al. [2012], methyl groups increase the hydrophobicity of OMPs. Therefore, it can be speculated that zeolites had higher adsorption capacity for more hydrophobic OMPs. This was consistent with the finding by [Jiang, 2019] that the higher hydrophobicity of the OMPs led to the higher adsorption capacity.

3.1.3 Effect of zeolite characteristics

The adsorption isotherm of OMPs by BEA and MOR were compared in Figure 3.4. In most cases, the adsorption capacity of MOR was higher than that of BEA, which was related to their characteristics. According to the zeolite characteristics listed in Table 2.1, the negative charged sites on BEA and MOR powders were neutralized by H^+ and the Brønsted acidic sites ($Si(OH)^+Al^-$) were generated. The higher Al^{3+} content results in more negative charges, and thus more Brønsted acidic sites [Jiang et al., 2018].

In our study, the Al^{3+} content of MOR is higher than that of BEA. Therefore, more acidic sites existed on the MOR zeolite. Moreover, research has shown that acidic sites may promote the adsorption of certain OMPs on high-silica zeolites due to specific interaction. For example, the results of Blasioli et al. [2014] indicated that sulfamethoxazole interacted with FAU and MOR zeolites by weak H-bonds. Therefore, it was hypothesized that the larger Al^{3+} content might be responsible for the higher adsorption capacity of MOR zeolite due to stronger H-bonding interaction between the OMPs molecules and Brønsted acidic sites on zeolite surface.

It is worth noting that BEA and MOR had different behaviors for the adsorption of carbamazepine. It was found in the literature that carbamazepine may form molecular chains of enlarged size due to the molecular interactions, while the molecular chain of carbamazepine could not enter the MOR and MFI zeolites with narrow chan-

nel openings [Martucci et al., 2012]. However, in our study, the removal capacity of MOR on carbamazepine was found to be much higher than that of BEA. Therefore, it can be speculated that the size of the molecule was not the main factor that affects the adsorption of carbamazepine. Furthermore, as carbamazepine is a neutral compound, the charge effect on the adsorption can also be excluded. Consequently, the explanation for the better removal of carbamazepine by MOR might be the stronger effect of the special bonding formed between carbamazepine and MOR zeolites, e.g. H-bonding.
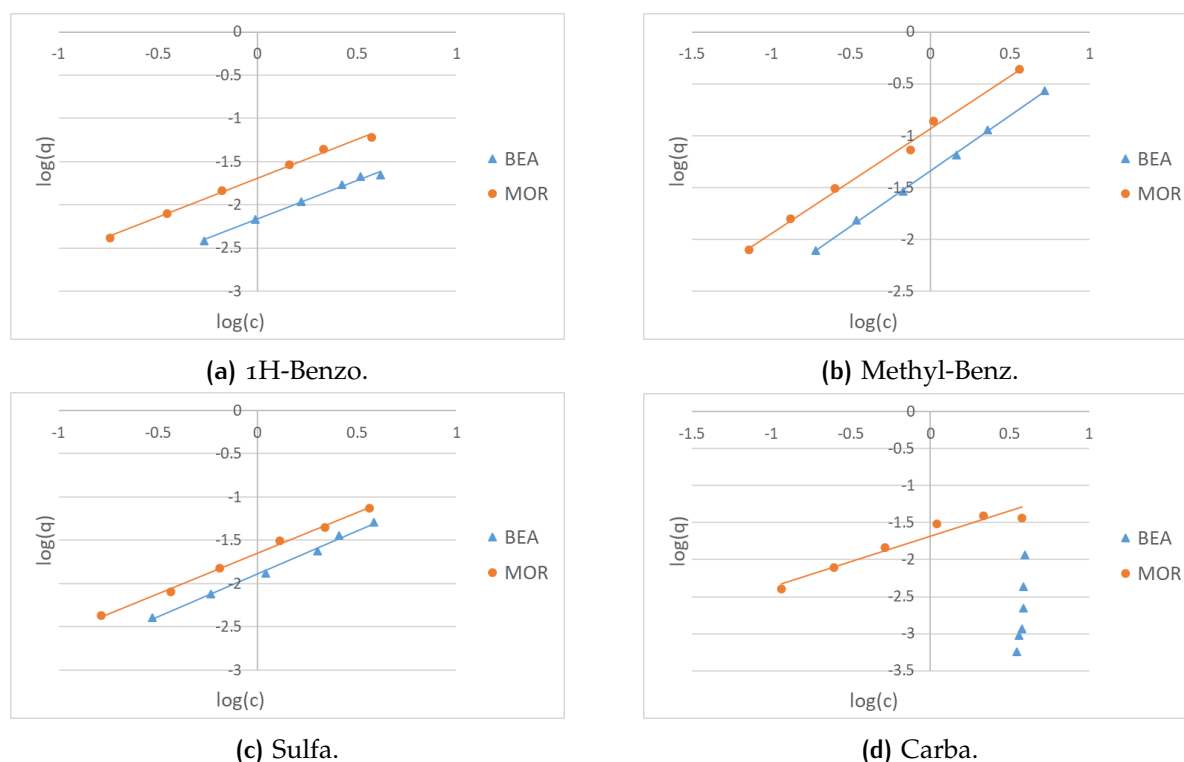

(a) 1H-Benzo.

(b) Methyl-Benz.

(c) Sulfa.

(d) Carba.

Figure 3.4: Adsorption isotherms of medium-removal OMPs in demi-water by BEA and MOR zeolite powders with Freundlich model fitting. Carbamazepine had no suitable isotherm in the BEA case, thus data points are shown without fitting

3.1.4 Effect of WW matrix

The adsorption isotherm of OMPs in WW and demi-water are plotted and compared in Figure 3.5. The yellow dots represent WW, the blue dots represent demi-water. At low zeolite dosages (from 1 to 50 mg/l), the adsorption capacity of OMPs in WW was minimal, resulting in the poor quality of the fitting. Thus, only 5 or 4 data points were plotted without fitting to isotherm model.

It can be seen from Table 3.1 that, in most cases, the performance of zeolites for OMP removal in WW was worse than that in demi-water, except for the better perfor-

mance of BEA for hydrochlorothiazide removal in WW, which might be due to the measurement bias for this compound. From Figure 3.5, it can be found that the adsorption capacity of 1H-benzotriazole, methyl-benzotriazol, sulfamethoxazole were obviously decreased in WW.
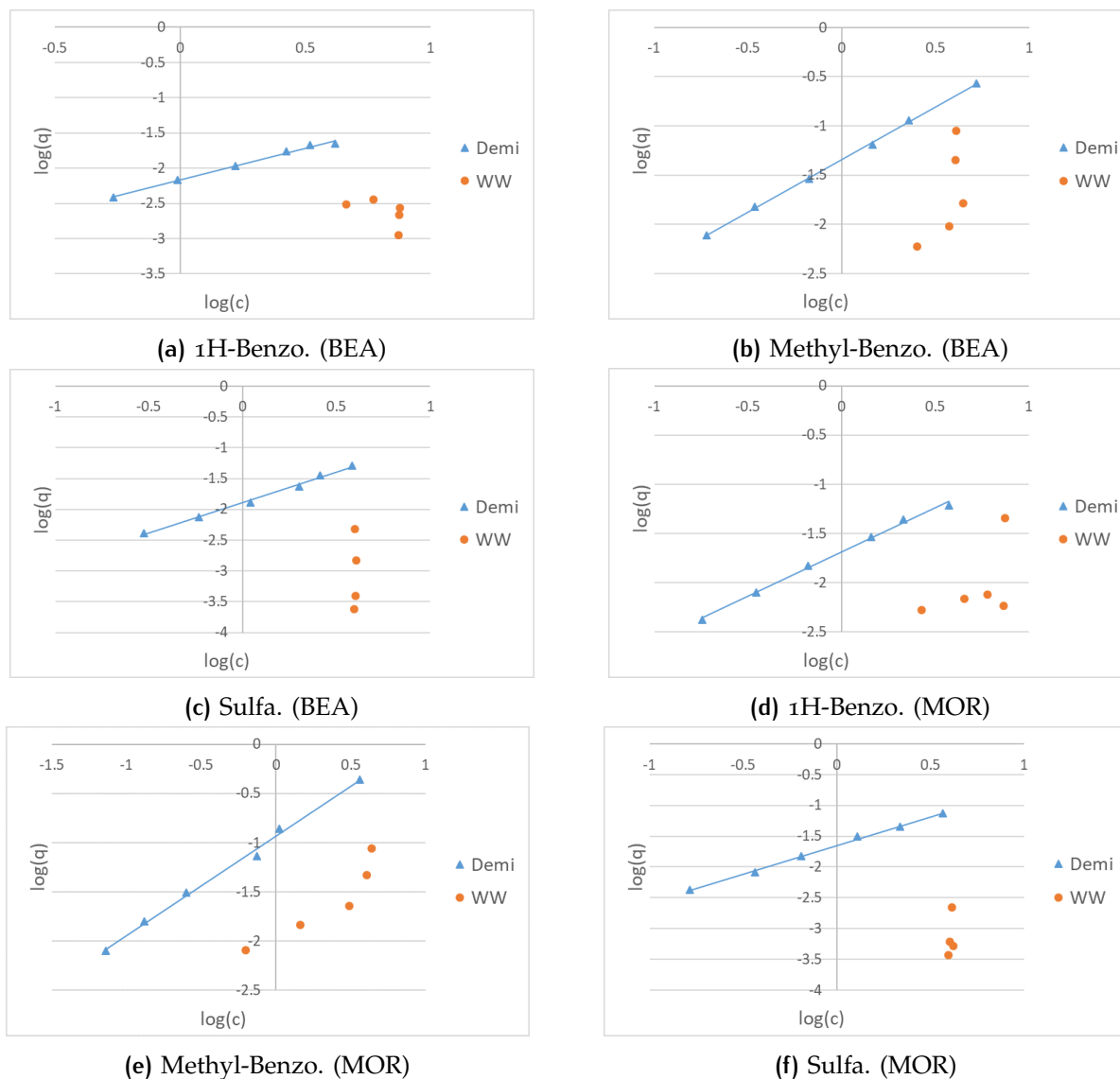

(a) 1H-Benzo. (BEA)

(b) Methyl-Benzo. (BEA)

(c) Sulfa. (BEA)

(d) 1H-Benzo. (MOR)

(e) Methyl-Benzo. (MOR)

(f) Sulfa. (MOR)

Figure 3.5: Adsorption isotherms of medium-removal OMPs in demi-water and WW by BEA and MOR zeolite powders

One reason for the reduced capacity might be that the presence of BOMs in the WW hindered the adsorption of OMPs by covering the surface of zeolites [De Ridder et al., 2012]. Moreover, a small portion of BOM fractions with low molecular weight would enter the micropores of the zeolites, and BOM competition with OMPs for the adsorption sites in the micropores were likely to happen [Jiang, 2019].

The differed pH of the WW might be another reason for the reduced capacity. The pH of WW was in the range of 8.0-8.2, which was higher than that of demi-water solution (pH 6.5). When the pH of the solution is higher than the pKa of OMPs' functional groups, the OMP molecules will be deprotonated, which may decrease the net charge of OMP molecules in solution. The decreased net charge resulted in weaker electrostatic attraction or stronger electrostatic repulsion between OMP molecules and negative zeolite surface, consequently, a reduced adsorption capacity. The same phenomenon was also observed in the research done by Tsai et al. [2006], that the adsorption capacity of bisphenol-A was reduced in the solution with higher pH.

3.2 ADSORPTION KINETICS OF OMPS BY ZEOLITE GRAN-ULES

The adsorption kinetic experiments were conducted at three zeolite dosages (i.e. 50 mg/L, 250 mg/L and 500 mg/L) to study the OMP adsorption rates by zeolite granules. In this section, the changing of OMP adsorption amounts over time were plotted with PFO fitting curves. The adsorption rate of different OMPs were compared. The differences of adsorption kinetics in demi-water and WW were demonstrated. In addition, the results of adsorption kinetics were fitted by IPD model to investigate the transport of OMPs during the process of adsorption by granules.

3.2.1 Adsorption kinetics in demi-water

Prior to the discussion, some special cases in the kinetic results should be mentioned.

- The kinetic results of propranolol, clarithromycin and hydrochlorothiazide by BEA and MOR zeolites were not available due to measurement errors.

- In the BEA kinetic tests, the equilibrium concentration of well adsorbed OMPs, i.e. trimethoprim, sotatol and metoprolol, decreased to zero at zeolite dosage of 250 mg/L and 500 mg/L, only the kinetics at 50 mg/L can be estimated. In the MOR kinetic tests, the equilibrium concentration of well adsorbed OMPs decreased to zero at all three dosages, thus were not displayed.

- The adsorption kinetics of OMPs with medium removal capacity, i.e. 1H-benzotriazole, methyl-benzotriazole and sulfamethoxazole, can be estimated at all three zeolite dosages.

- For carbamazepine and diclofenac which were poorly adsorbed, the decrease of concentrations at zeolite dosages of 50 and 250 mg/L were not significant, only the adsorption kinetics at 500 mg/L were plotted.

Plotting of kinetic data

The OMP adsorption kinetics by BEA and MOR zeolite granules at three zeolite dosages are plotted in Figure 3.6 and Figure 3.7, respectively. The kinetic curves can be grouped according to the OMP removal capacity. The red arrows in the figures indicate the increase or decrease trend of the adsorption loading of each group after 400h. One thing should be noticed is that the adsorption loading of methyl-benzotriazole (medium-removal) by BEA zeolite was higher than the good-removal OMPs, which was due to the unexpectedly two times high initial concentration of this compound. The initial concentrations of the other OMPs were ~4 µg/L.
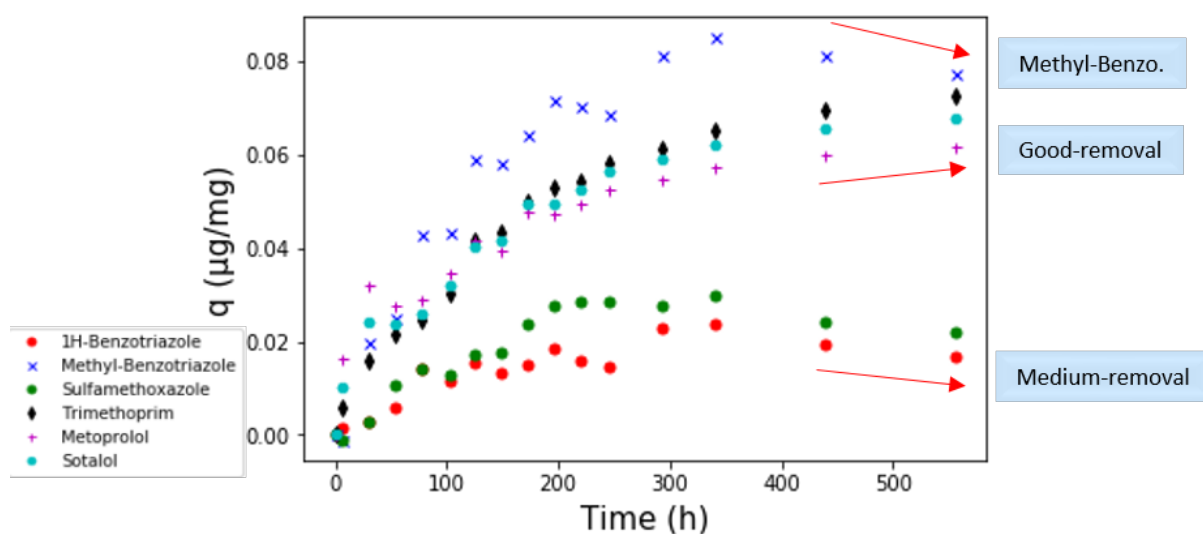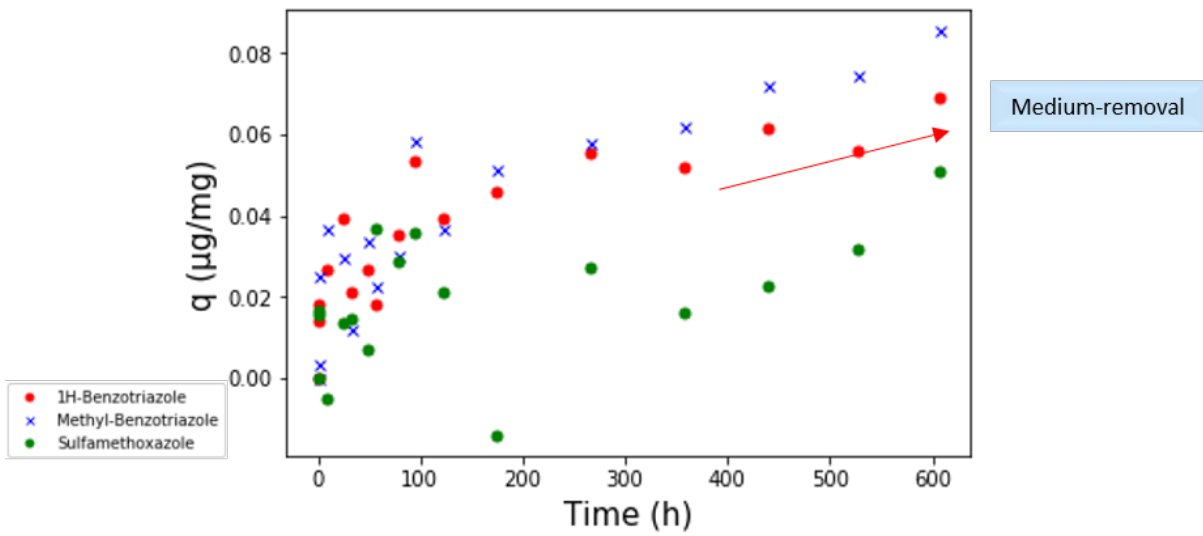

(a) BEA dosage 50 mg/L
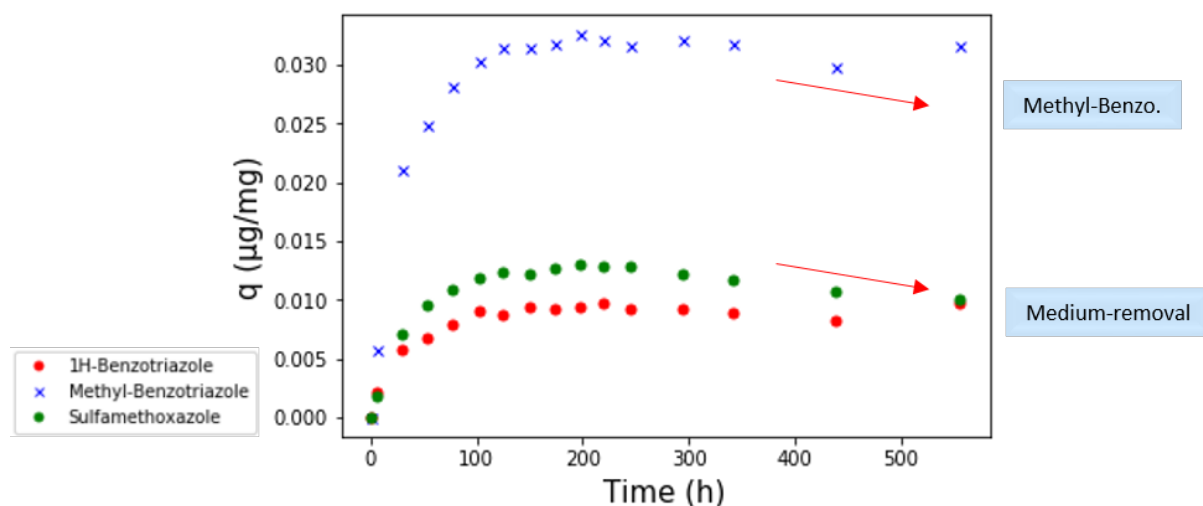
(b) BEA dosage 250 mg/L
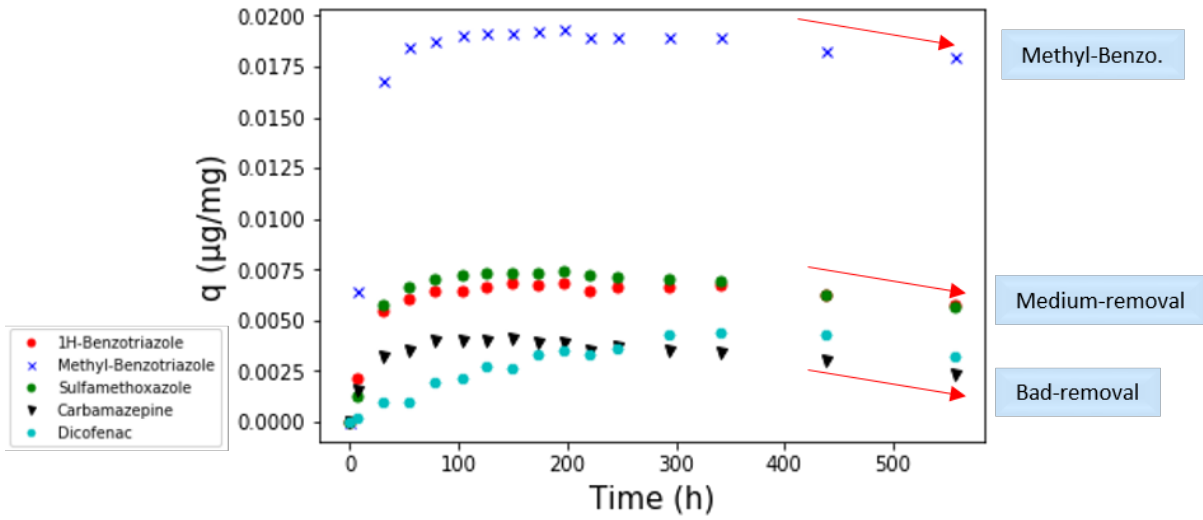
(c) BEA dosage 500 mg/L

Figure 3.6: OMP adsorption kinetics by BEA granules at zeolite dosages of (a) 50, (b) 250 and (c) 500 mg/L

(a) MOR dosage 50 mg/L

(b) MOR dosage 250 mg/L
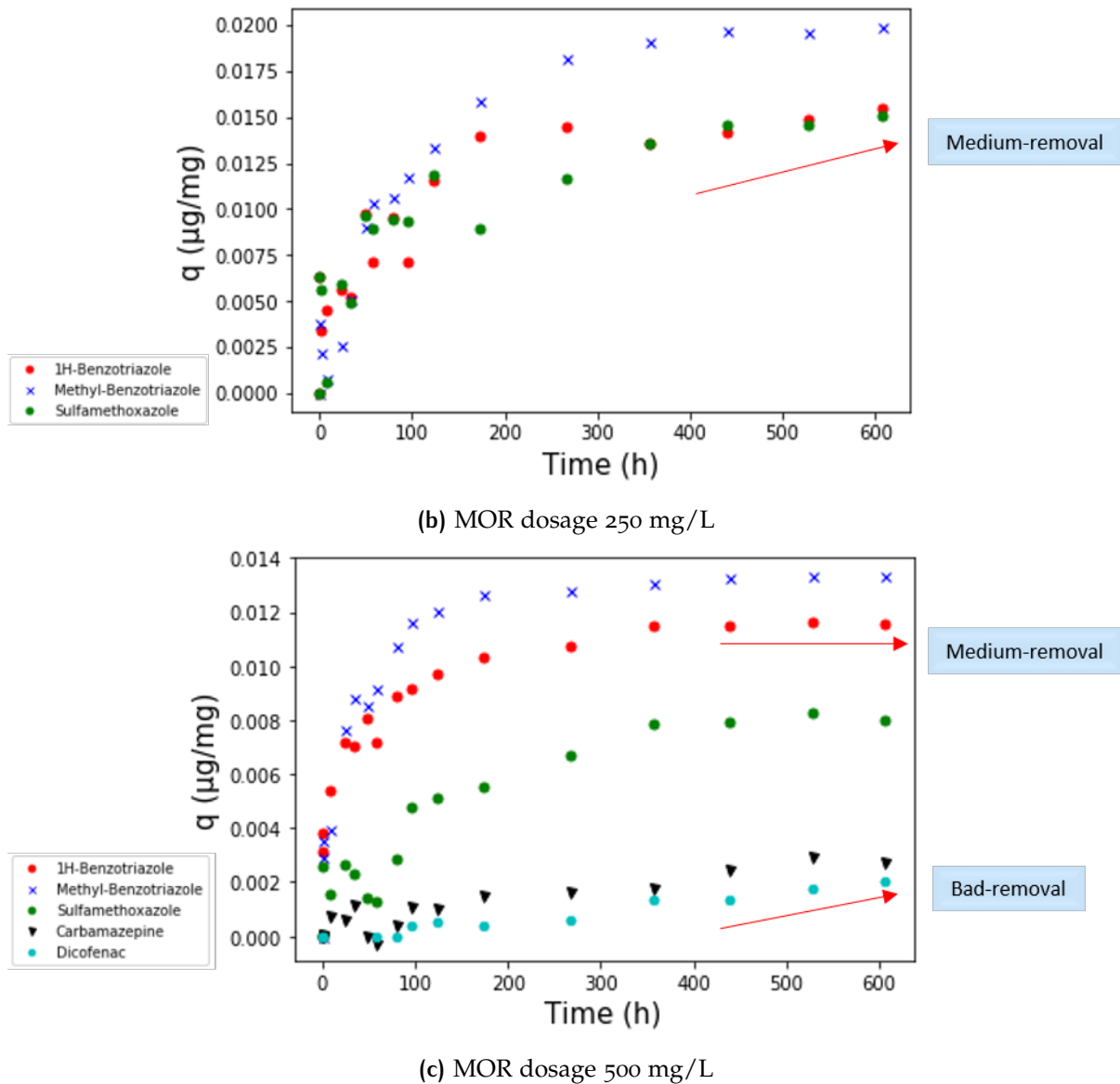

(c) MOR dosage 500 mg/L

Figure 3.7: OMP adsorption kinetics by MOR granules at zeolite dosages of (a) 50, (b) 250 and (c) 500 mg/L

From the BEA kinetics shown in Figure 3.6, downward trends after 400h can be observed from the adsorption loading of medium and bad-removal OMPs, including 1H-benzotriazole, methyl-benzotriazole, sulfamethoxazole, carbamazepine and diclofenac. However, the adsorption loading of good-removal OMPs, i.e. trimethoprim, sotatol and metoprolol, increased during the whole experiment period.

One possible explanation for the observation can be that, the medium and bad-removal OMPs were firstly adsorbed by zeolite, afterwards, the adsorbed molecules were replaced by OMPs that were well adsorbed, resulting in the desorption of the former. The phenomenon of OMP desorption from adsorbent was also reported in

literature [Sharma et al., 2013; Halder et al., 2016]. Sharma et al. [2013] studied the adsorption of cationic dye from aqueous solution using graphene oxide nanosheets, the thermodynamic calculation results indicated that the process was governed by physical adsorption due to electrostatic interaction between adsorbate-adsorbent species along with the π- πinteraction, and the dye molecules tended to revert back to the solution after attaining equilibrium.

From the MOR kinetics shown in Figure 3.7, the data of 1H-benzotriaz-ole, methyl-benzotriazole and sulfamethoxazole reached the plateau after 400h at zeolite dosage of 500 mg/L. However, the adsorption loading of these three OMPs kept increasing after 400h at dosages of 50 mg/L and 250 mg/L. This indicated that it took more time for OMPs to reach the adsorption equilibrium at a lower zeolite dosage. Besides, it can be found that the adsorption loading of carbamazepine and diclofenac kept increasing after 25 days even at high dosage of 500 mg/L, and it took more time for OMPs to reach equilibrium by MOR granules than BEA granules. The slower kinetics of MOR might be due to the larger size of MOR granules. The comparison between BEA and MOR kinetics will be further discussed in Section 3.2.2.

PFO model fittings

As mentioned in Section 2.3.3, the values of q_e in the kinetic data fitting were determined in two ways:

Method 1: with powder q_e, calculated from OMP adsorption isotherms by zeolite powders.

Method 2: with granule q_e, obtained by fitting the results of OMP adsorption kinetics by zeolite granules.

These two methods led to different kinetic constants. There were no isotherms for good-removal and bad-removal OMPs. Thus, in those two cases, the q_e values were determined by Method 2. The PFO fitting of OMP kinetics in demi-water by BEA and MOR zeolites are displayed in Figure D.1 and Figure D.2 (Appendix D), respectively. The obtained PFO kinetic parameters for BEA and MOR are displayed in Table 3.3 and Table 3.4, respectively.

Table 3.3: PFO fitting constants for OMP adsorption in demi-water by BEA granules

Name	Dosage (mg/L)	Method 1 with powder q_e			Method 2 with granule q_e		
		q_{e1} (μg/g)	k_1 (1/h)	R^2	q_{e2} (μg/g)	k_2 (1/h)	R^2
1H-Benzo.	50	21.12	8.36E-03	0.88	20.10	9.37E-03	0.88
	250	11.70	1.17E-02	0.64	9.21	2.94E-02	0.98
	500	7.34	3.83E-02	0.84	6.51	6.12E-02	0.98
Methyl-benzo.	50	149.14	2.60E-03	0.76	84.06	8.35E-03	0.98
	250	39.56	1.34E-02	0.69	31.68	3.25E-02	0.99
	500	20.80	5.10E-02	0.90	18.91	7.07E-02	1.00
Sulfa.	50	34.05	5.93E-03	0.85	28.02	9.06E-03	0.90
	250	14.40	1.70E-02	0.77	12.10	3.02E-02	0.96
	500	7.90	3.48E-02	0.83	7.02	5.04E-02	0.95
Trime.	50	-	-	-	75.26	5.91E-03	0.99
Sotalol.	50	-	-	-	67.85	7.08E-03	0.96
Metop.	50	-	-	-	57.92	1.02E-02	0.87
Carba.	500	-	-	-	3.62	8.71E-02	0.84
Diclo.	500	-	-	-	4.19	7.97E-03	0.94

Table 3.4: PFO fitting constants for OMP adsorption in demi-water by MOR granules

Name	Dosage (mg/L)	Method 1 with powder q_e			Method 2 with granule q_e		
		q_{e1} (μg/g)	k_1 (1/h)	R^2	q_{e2} (μg/g)	k_2 (1/h)	R^2
1H-Benzo.	50	50.42	2.01E-02	0.62	60.77	1.25E-02	0.71
	250	14.13	1.48E-02	0.79	15.00	1.29E-02	0.80
	500	11.90	2.29E-02	0.75	10.82	3.20E-02	0.79
Methyl-benzo.	50	108.06	2.98E-03	0.66	78.09	7.44E-03	0.78
	250	21.26	8.51E-03	0.96	19.89	9.84E-03	0.97
	500	13.46	2.52E-02	0.91	12.90	2.84E-02	0.92
Sulfa.[a]	50	53.8	-	-	44.01	-	-
	250	23.4	-	-	11.85	-	-
	500	11.07	3.26E-03	0.84	8.54	6.37E-03	0.92
Carba.	500	8.99	6.72E-04	0.89	4.65	1.70E-03	0.90
Diclo.	500	-	-	-	4.00	1.06E-03	0.93

[a] The PFO model can not estimate the kinetic constants for sulfamethoxazole at dosage of 50 mg/L and 250 mg/L due to relatively poor data quality. q_{e2} was determined manually.
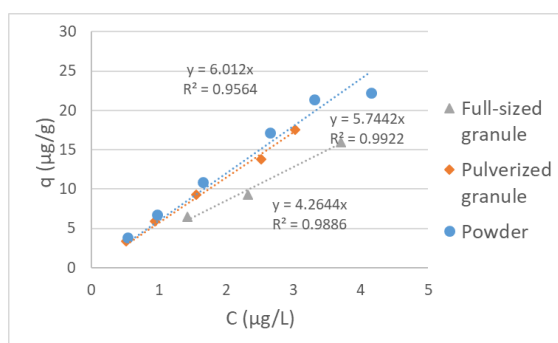
kinetic constants

In this study, it was found that the kinetic constant k varied with zeolite dosages. This phenomenon was also reported by Ho and Chiang [2001] and Tsai et al. [2006]. According to Chu [2010], when mass transfer limitation is present, the rate constants are no longer the intrinsic rate constants but lumped rate constants containing the effects of both the intrinsic kinetics and mass transport. In our case, the kinetic constant in the PFO model was a lumped parameter representing both external and internal transport processes. It was hypothesised that the water film wrapped around the zeolite particles can change due to different hydraulic conditions at different dosages, so the external diffusion of the solute might be affected, resulting in different k values.
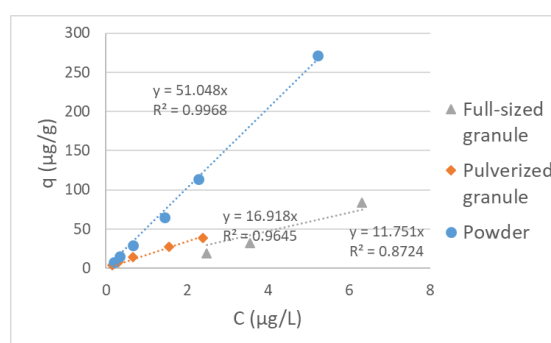
Granule isotherms

From Table 3.3 and Table 3.4, it can be found that, in most cases, the actual equilibrium loading (q_{e2}) estimated by the granule kinetics (Method 2) was lower than the theoretical equilibrium loading (q_{e1}) calculated by powder isotherms (Method 1). Thus, OMP adsorption capacity by zeolite granules was expected to be lower than the capacity by zeolite powders.

Based on the estimated equilibrium loading (q_{e2} in Table 3.3 and Table 3.4) at three zeolite dosages, the three-point isotherms by BEA and MOR granules can be plotted. In addition, the isotherm of pulverized granules were provided by Nan Jiang. In the experiments, the full-sized granules were pulverized into smaller particles with a sieve size of 0.355-0.85 mm, and the duration of the isotherm test was 14 days. The linear isotherm fitting of powder, full-sized granule and pulverized granule for the three medium-removal OMPs are compared in Figure 3.8. The linear isotherm constants K_L are summarized in Table 3.5.

(a) 1H-Benzo.(BEA)

(b) Methyl-Benzo. (BEA)

(c) Sulfa. (BEA)

(d) Benzo. (MOR)
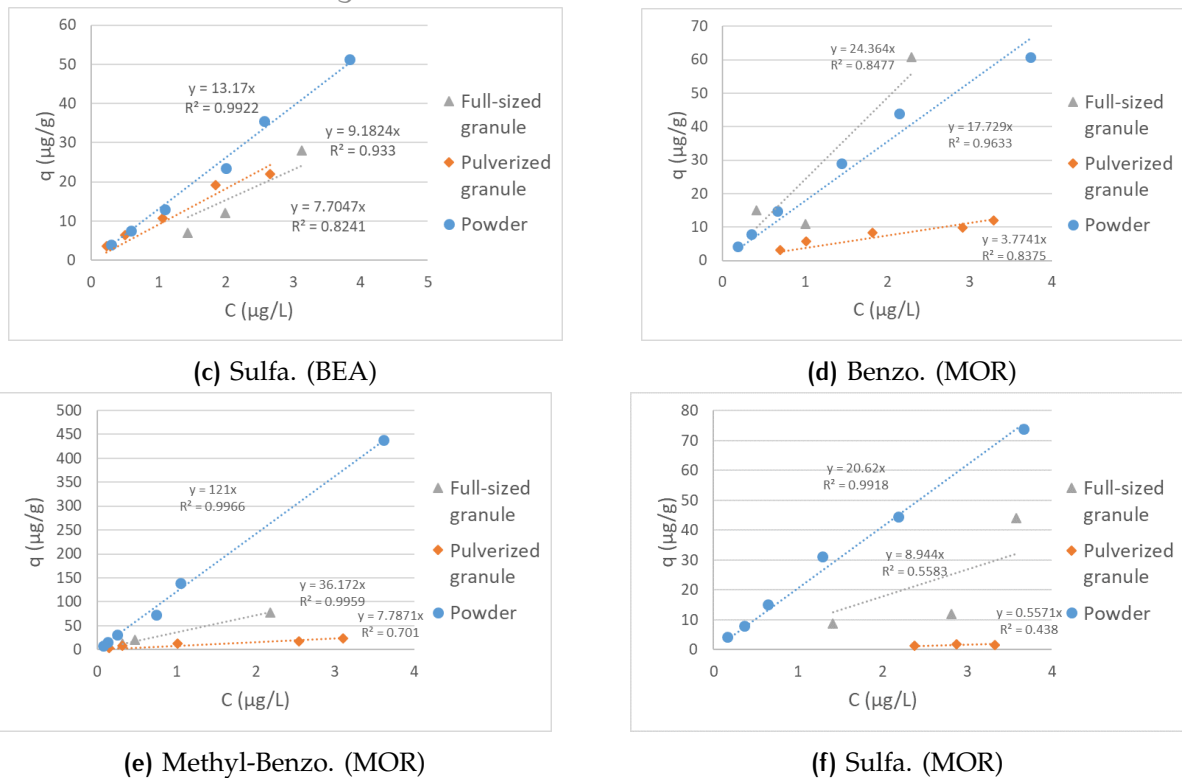
(e) Methyl-Benzo. (MOR)

(f) Sulfa. (MOR)

Figure 3.8: The linear adsorption isotherms of medium-removal OMPs in demi-water by powders, pulverized granules, and full-sized granules of BEA and MOR zeolites

A higher value of K_L means a higher adsorption capacity. From Figure 3.8, full sized granules and pulverized granules showed lower adsorption capacities than that of powders in most cases. OMP adsorption capacities by BEA zeolites follow the order of powder >pulverized granule >full-sized granule. It indicated that, in most cases, the inside of the full-size granules was not fully utilized within the 25-day equilibrium time.

However, it can be found in the case of MOR, where the pulverized granule showed lower capacity than the full sized granule. Possible reason was that the equilibrium of the pulverized MOR granules might not be achieved. Moreover, MOR granule had higher adsorption capacity for 1H-benzotriazole than powder, which might be due to the relatively poor fitting quality of the granule data for 1H-benzotriazole. In the future study, the adsorption equilibrium time must be extended for full sized granules and pulverized granules experiments with more zeolite dosages are needed to ensure the accuracy of results.

Table 3.5: K_L[a] for powder, full sized granule and pulverized granule in demi-water

	BEA			MOR		
	1H-Benzo.	Methyl-Benzo.	Sulfa.	1H-Benzo.	Methyl-Benzo.	Sulfa.
K_L for powder (*0.85)	5.1	43.4	11.2	15.0	102.9	17.5
K_L for full sized granule	4.3	11.8	7.7	24.3	36.2	8.9
K_L for pulverized granule	5.7	16.9	9.2	3.8	7.8	0.6

[a] Unit of K_L: m^3/kg

3.2.2 Adsorption rate comparing

In order to compare the adsorption rates of different OMPs, one should refer to the rate described by Equation 3.1 instead of just looking at the kinetic constant k_{PFO}. The adsorption rate (dq/dt) is changing over time, and is determined by both the rate constant k_{PFO} and the driving force (q_e-q_t) [Wang and Guo, 2020].

$$PFO_{rate} = k_{PFO}(q_e - q_t) \tag{3.1}$$

where k_{PFO} is the PFO kinetic constant (1/h), q_e is the adsorption equilibrium loading (µg/mg), q_t (µg/mg) is the adsorption loading at time t.

Assuming q_t to be 1 µg/g for all OMPs, together with the method 2 q_e and corresponding k_{PFO} from Table 3.3, the PFO_{rate} were calculated for each compound at dosage of 500 mg/L (medium and bad-removal) or 50 mg/L (good-removal). The results are listed in Table 3.6.

Table 3.6: PFO rate comparison for OMP adsorption kinetics in demi-water by BEA and MOR granules

Name	Dosage (mg/L)	BEA dq/dt ((µg/g)/h)	MOR dq/dt ((µg/g)/h)
1H-Benzo.	500	337.62	314.51
Methyl–benzo.[a]	500	1265.77	338.58
Sulfa.	500	303.42	48.04
Trime.	50	438.96	-
Sotalol.	50	473.29	-
Metop.	50	579.40	-
Carba.	500	227.92	6.21
Diclo.	500	25.44	3.18

[a] The initial concentration of methyl-benzotriazole in the BEA case was twice higher than the others, resulting in a higher PFO rate. Therefore, methyl-benzotriazole was not involved in PFO rate comparing.

According to the data of BEA, it can be found that the good-removal OMPs had higher PFO rates ranging from 400-600 ((μg/g)/h). The medium-removal OMPs had lower PFO rates, which were 337.62 ((μg/g)/h) for 1H-benzotriazole, and 303.42 ((μg/g)/h) for sulfamethoxazole. The PFO rate of bad-removal OMPs was smaller than the others, and diclofenac had the smallest PFO rates among all the OMPs. The order of BEA kinetics can be summarized: metoprolol >sotalol >trimethoprim >1H-benzotriazole >sulfamethoxazole >carbamazepine >diclofenac.

The PFO rates of MOR were generally smaller than that of BEA, which can be the reason for the slower equilibrium in the MOR kinetics tests (Figure 3.7). According to Heijman et al. [2002], the adsorption rate is higher with smaller grain size, hence, the larger granule size of MOR should be responsible for its lower kinetics. Remarkably, the PFO rate of sulfamethoxazole and carbamazepine were small compared to the other OMPs by MOR, regardless of the relatively high adsorption capacity of sulfamethoxazole and carbamazepine. The order of MOR kinetics can be summarized: methyl-benzotriazole >1H-benzotriazole >sulfamethoxazole >carbamazepine >diclofenac.

It is worth noticing that the q_e used in the rate comparison were affected by the initial concentration C_0. In order to make comparisons on the rates, C_0 should be kept the same for all OMPs during the kinetic experiment.

3.2.3 Adsorption kinetics in WW

OMP adsorption kinetics in demi-water and WW by BEA zeolites were plotted in Figure E.1 (Appendix E) with PFO fitting curves. The PFO fitting constants by BEA zeolite can be found in Table 3.7. Due to the background concentration of OMPs in WW, the C_0 of all OMPs in the spiked WW solution were 0.4-3 μg/L higher than that of demi-water solution. A differed C_0 could add uncertainty to the comparison on PFO rates, which should be specifically noted during the comparison process.

Table 3.7: PFO fitting constants for OMP adsorption in demi-water and WW by BEA granules

Name	Dosage (mg/L)	Demi-water q_e (μg/g)	k_1 (1/h)	R^2	WW q_e (μg/g)	k_1 (1/h)	R^2
1H-Benzo.[a]	500	6.51	6.12E-02	0.98	9.38	2.98E-02	0.96
Methyl-benzo.	500	18.91	7.07E-02	1.00	17.82	3.33E-02	0.96
Sulfa.	500	7.02	5.04E-02	0.95	1.93	3.41E-02	0.81
Trime.	50	75.26	5.91E-03	0.99	49.55	6.55E-03	0.98
Sotalol.[a]	50	67.85	7.08E-03	0.96	79.34	6.12E-03	0.99
Metop.[a]	50	57.92	1.02E-02	0.87	101.86	6.20E-03	1.00
Propra.	50	-	-	-	75.16	6.31E-03	0.99
Carba.[b]	500	3.62	8.71E-02	0.84	-	-	-
Diclo.	500	4.19	7.97E-03	0.94	5.55	1.28E-02	0.96

[a] Higher q_e in WW due to higher C_0.
[b] The removal of cabamazepine in WW was minimal, so the PFO model can not be well fitted.

Table 3.8: PFO rate comparison for OMP adsorption kinetics in demi-water and WW by BEA granules

Name	Dosage (mg/L)	Demi-water dq/dt ((μg/g)/h)	WW dq/dt ((μg/g)/h)
1H-Benzo.	500	337.62	249.83
Methyl–benzo.	500	1265.77	560.10
Sulfa.	500	303.42	31.54
Trime.	50	438.96	317.82
Sotalol.	50	473.29	479.06
Metop.	50	579.40	625.18
Propra.	50	-	468.04
Carba.	500	227.92	-
Diclo.	500	25.44	58.25

As shown in Table 3.8, the two good-removal OMPs, i.e. metoprolol and sotatol, showed higher PFO rate in WW than in demi-water, which was due to the higher C_0 in WW.

Despite the higher C_0 of trimethoprim, 1H-benzotriazole, methyl-benzotriazole and sulfamexazole, the PFO rates of these compound were lower in WW. The pH effect of WW and the pore blocking effect by the BOMs might be responsible for the decrease.

It can be found that the calculated adsorption rate for diclofenac was higher in WW, the higher PFO rate of this compound can also be attributed to the higher C_0. As the pKa value of diclofenac is 4, the net charge of diclofenac molecules was not changed from demi-water pH (6.5) to WW pH (8.2), hence, the charge effect on the different adsorption behavior can be excluded. After excluding the charge effect, it can be inferred that the pore blocking effect of BOMs was not enough to cause a decrease on the kinetic rate of diclofenac.

3.2.4 Intra-particle diffusion model fitting

To further investigate the transport of OMPs during the adsorption processes, the IPD model was used to fit the BEA kinetic data by plotting q_t versus $t^{0.5}$. The adsorption kinetics of medium-removal and bad-removal OMPs at zeolite dosage of 500 mg/L, as well as the adsorption kinetics of good-removal OMPs at zeolite dosage of 50 mg/L were fitted to IPD model; kinetics in demi-water was studied. IPD fitting curves were shown in Figure 3.9.

Four sections can be identified from OMPs, including 1H-benzotriazole, methyl-benzotriazole, sulfamexazole and carbamazepine, indicating that four periods might be involved in the adsorption process of these OMPs [Kalavathy et al., 2005; Hameed and El-Khaiary, 2008]. Section 1 (sec 1) could be the film diffusion. In the initial stage, OMP molecules had to pass through the liquid boundary layer surrounding the zeolite granules [McKay et al., 1985]. The second section (sec 2) represented intra-particle diffusion, in which OMPs entered the inner pores of zeolite granules and was adsorbed onto the internal adsorption sites [Zhang et al., 2019]. The third section (sec 3) was the equilibrium stage where intra-particle diffusion started to slow down [Wu et al., 2005]. The fourth section (sec 4) was the desorption of the OMP molecules, where the OMPs were released back to the solution. It can be noticed that only two data points were identified in the first section, which means that the actual transition between the film diffusion and the intra-particle diffusion could have occurred before the second data point.

For diclofenac (Figure 3.9e), only three sections were identified. As the film diffusion was proven to exist in the other OMPs, the first section in the diclofenac data should also be the film diffusion; intra-particle diffusion of this compound was then negligible. The following two sections were the equilibrium and the desorption stages. Accordingly, it can be inferred that diclofenac was preferably adsorbed on the surface of the zeolite instead of entering the pores.

The data of good-removal OMPs, i.e. metoprolol, sotalol, and trimethoprim showed two sections. The first section should be the film diffusion and the second should
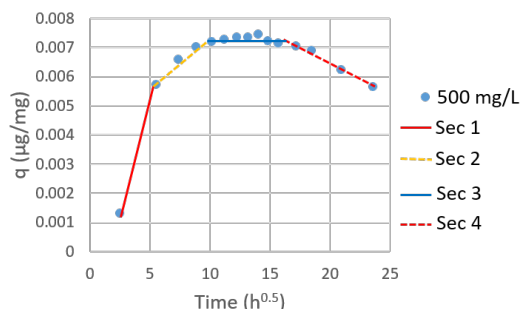
be the intra-particle diffusion. In these cases, the adsorption equilibrium was not reached, so the third and fourth sections were not found.
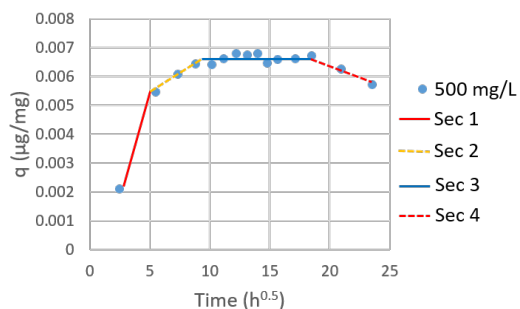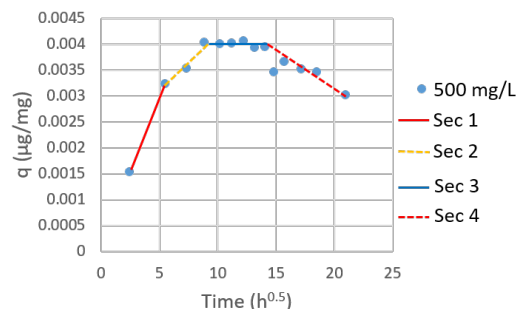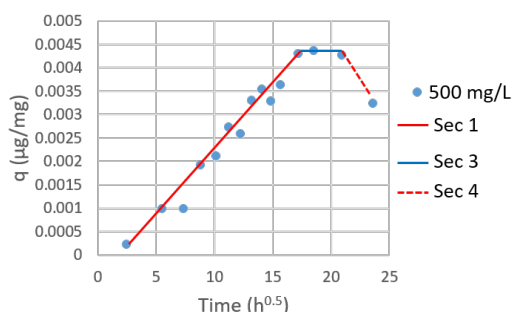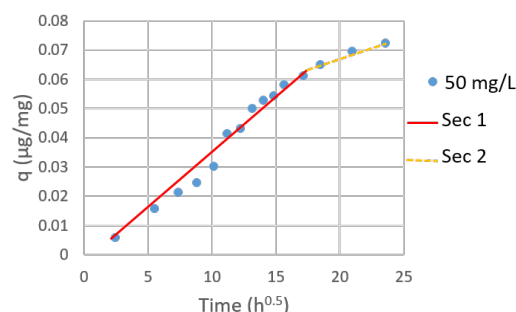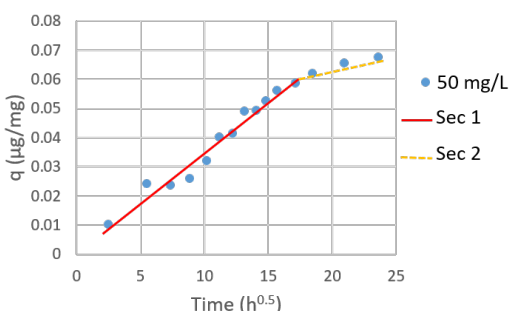

(a) 1H-Benzo.
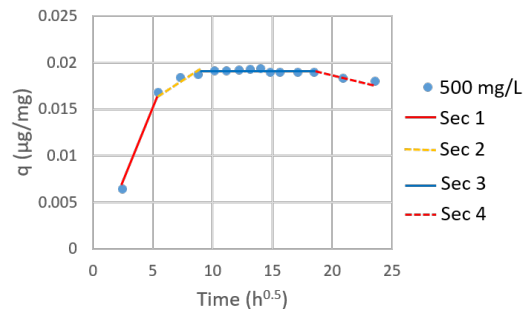
(b) Methyl-Benzo.

(c) Sulfa.

(d) Carba.
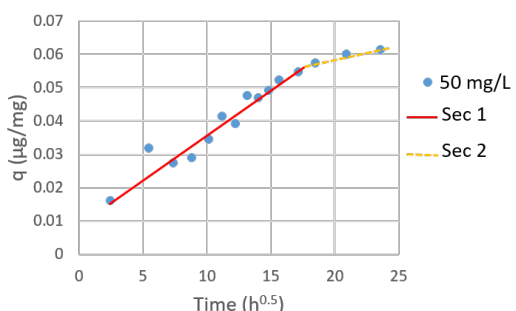
(e) Diclo.

(f) Trime.

(g) Sotalol.

(h) Metop.

Figure 3.9: IPD fitting curves for OMP adsorption kinetics by BEA granules

3.3 BREAKTHROUGH CURVES IN COLUMN EXPERIMENTS

Column experiments were conducted with BEA and MOR zeolite granules. The operating parameters are listed in Table 2.4. In this section, factors that affected the breakthrough behaviour will be discussed, including the adsorption capacity and kinetics of OMPs, the zeolite characteristics and the EBCT.

3.3.1 Effect of adsorption capacity and kinetics of OMPs

The breakthrough curves of OMPs at EBCT 20 min are plotted in Figure 3.10. Propranolol, clarithromycin and hydrochlorothiazide were not well measured and were not presented. OMPs can be divided into three categories: (1) carbamazepine and diclofenac with significant breakthrough, (2) 1H-benzotriazole, methyl-benzotriazole and sulfamethoxazole with medium breakthrough, (3) metoprolol, sotalol, propranolol and trimethoprim with no obvious breakthrough.

The breakthrough percentage of medium and bad-removal OMPs in the BEA column followed the order of: diclofenac >carbamazepine >sulfamethoxazole >1H-benzotriazole >methyl-benzotriazole. In the MOR column, Diclofenac, carbamazepine and sulfamethoxazole had similar breakthrough curves, so the sequence of these three OMPs cannot be determined. The order of breakthrough percentage in column experiments, and the order of adsorption capacity and kinetics in batch experiments for OMPs are summarized in Table 3.9.

(a) BEA   (b) MOR
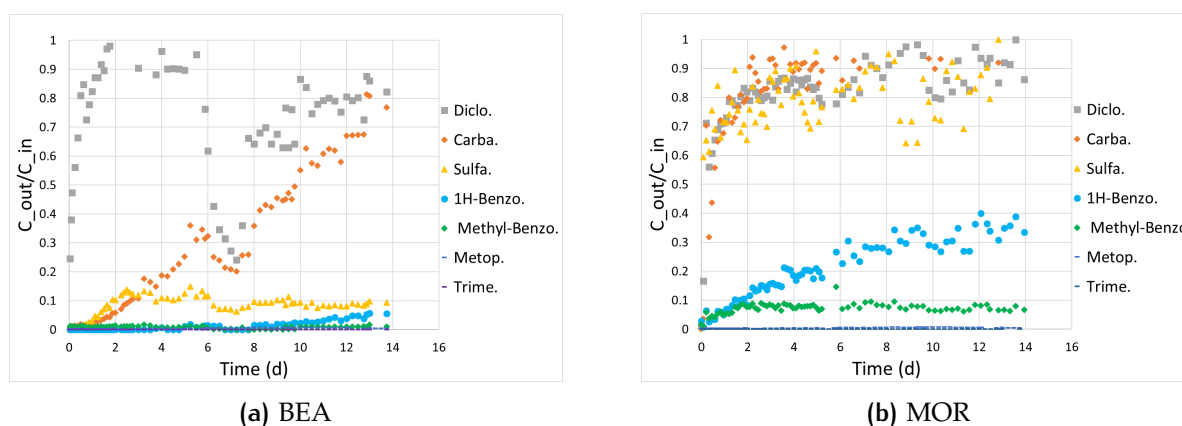
Figure 3.10: Breakthrough curves of OMPs in BEA and MOR columns at 20 min EBCT

Table 3.9: The order of adsorption capacity, kinetics and breakthrough in demi-water

		Order
BEA	Capacity	Methyl-benzo.>Sulfa.>1H-benzo.
	Kinetics	1H-benzo.>Sulfa.>Carba.>Diclo.
	Breakthrough %	Methyl-benzo.<1H-benzo.<Sulfa.<Carba.< Diclo.
MOR	Capacity	Methyl-benzo.>Carba.>Sulfa.>1H-benzo.
	Kinetics	Methyl-benzo.>1H-benzo.>Sulfa.>Carba.>Diclo.
	Breakthrough %	Methyl-benzo.<1H-benzo.<Sulfa.≈Carba.≈ Diclo.

* The OMPs marked in red are in reverse order in capacity and kinetics.

The OMP breakthrough in the column was firstly determined by the adsorption capacity of OMPs: the good-removal OMPs showed slow breakthrough, while the bad-removal OMPs showed fast breakthrough. In addition, it was noticed that the order of breakthrough percentage of medium-removal OMPs was consistent with the reverse order of the kinetic rate (marked in red in Table 3.9). Especially, carbamazepine and sulfamethoxazole with medium adsorption capacity by MOR still showed faster breakthrough in the MOR colum. Therefore, it can be summarized that the breakthrough of OMPs in the column was determined both by their adsorption capacity and kinetics. Furthermore, the breakthrough of OMPs with similar adsorption capacity by zeolites were mainly affected by the adsorption kinetics .

3.3.2 Effect of zeolite characteristics

The breakthrough curves of OMPs in BEA and MOR columns were compared in Figure 3.11. It can be found that BEA column had better OMP adsorption efficiency than MOR column when the EBCTs were the same. The reason can be that the kinetics of MOR was slower than that of BEA due to bigger granule size, and slower kinetics led to faster breakthrough. Moreover, the column of BEA and MOR were filled by packing the same height of zeolite granules. Since the density of MOR granule was almost half of the density of BEA granules, the weight of MOR granules was then half that of BEA granule (Table 2.4), which can also result in faster breakthrough.

(a) Carba.

(b) Diclo.

(c) 1H-Benzo.

(d) Methyl-Benzo.

(e) Sulfa.

(f) Metop.

(g) Sota.

(h) Trime.

Figure 3.11: Breakthrough curves of OMPs in demi-water by BEA and MOR columns at EBCT of 6 min and 20 min

3.3.3 Effect of EBCT

As shown in Figure 3.11, columns with 20 min EBCT had better removal efficiency for OMPs than the columns with 6 min EBCT, which was indicated by the smaller slope of the OMP breakthrough curves. It can be inferred that longer EBCT led to better OMP adsorption efficiency of the column. As OMP breakthrough was related to the adsorption kinetics of OMPs, longer EBCT enabled the better adsorption of OMPs with slower kinetics.

An obvious drop between the 6th and 8th day can be observed in BEA column with 20 min EBCT, which were marked in Figure 3.11a and Figure 3.11b. It was caused by the unexpected stop of inflow and outflow between the 6th and 8th day with on-going sample collection. The flow was opened afterwards and the outflow concentration increase again.

3.4 PREDICTION OF OMP BREAKTHROUGH CURVES

In this section, the breakthrough modelling results will be compared with the results in the column experiments; the sensitivity of the model to several important parameters will be discussed.

3.4.1 Dispersion coefficients

The dispersion coefficients (D_L) were measured by feeding NaCl solution to the column. The change of the conductivity of the outflow with time were plotted in Figure 3.12. The dispersion coefficients of MOR and BEA columns are listed in Table 3.10.

Table 3.10: Dispersion coefficients at different flow velocities

	1.67 cm/min	0.5 cm/min	Unit
BEA	3.00E-06	1.00E-06	m²/s
MOR	6.00E-06	1.30E-06	m²/s

(a) BEA (v=1.67 cm/min, D_L = 3E-6 m²/s)

(b) BEA (v=0.5 cm/min, D_L = 1E-6 m²/s)

(c) MOR (v=1.67 cm/min, D_L = 6E-6 m²/s)

(d) MOR (v=0.5 cm/min, D_L = 1.3E-6 m²/s)
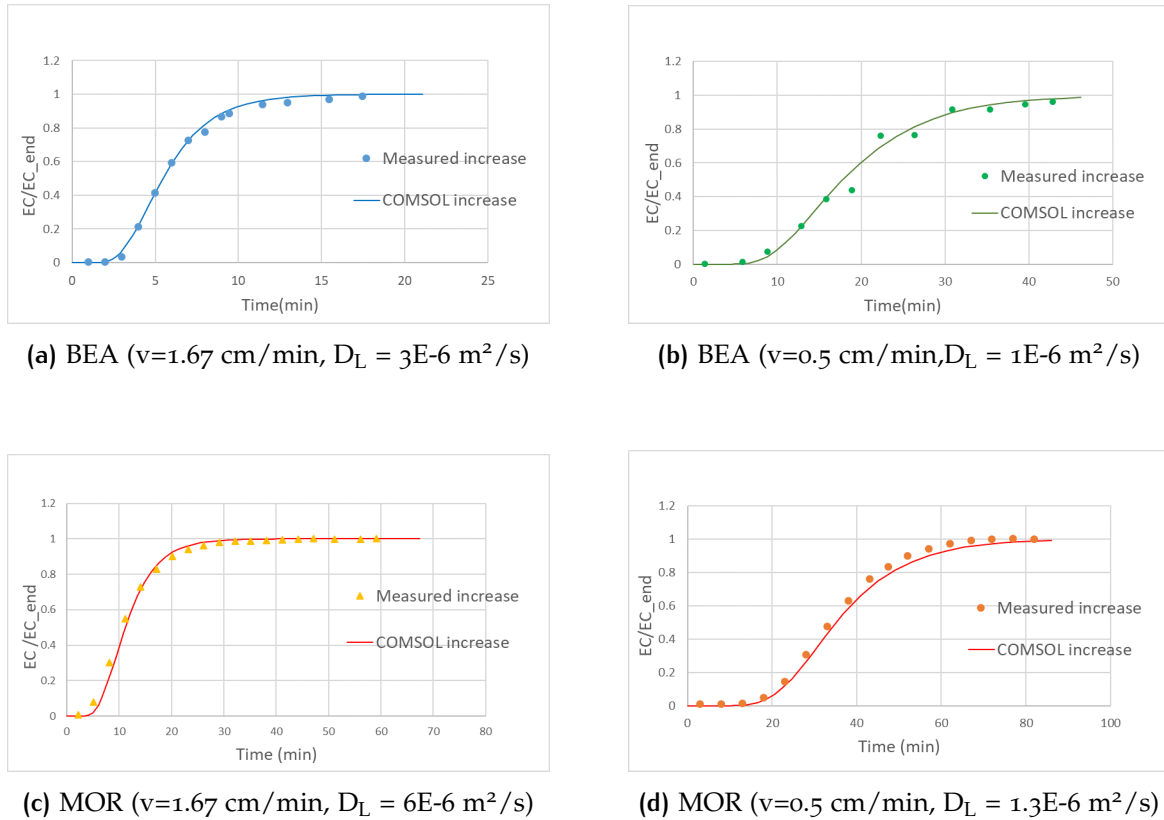
Figure 3.12: Breakthrough curves of NaCl in BEA and MOR columns under different flow velocities

The measured D_L was in the magnitude of 10^{-6} m²/s. Under the same flow velocity, D_L of MOR column was greater than that of BEA column, which was due to the larger porosity in the MOR columns as the granule size was bigger. D_L was also affected by the flow velocity that a faster velocity led to a greater D_L.

3.4.2 Breakthrough modelling

In the breakthrough model, three OMPs with medium removal capacities, i.e. 1H-benzotriazole, methyl-benzotriazole and sulfamethoxazole, with both isotherm and kinetic parameters from batch experiments were selected as target OMPs. As mentioned in the previous section, there were three types of isotherm parameters available in this study: isotherms from powders (Freundlich), three-point isotherm from full-size granules (linear) and isotherm from pulverized granule (linear). Two types of kinetic constants were available: one estimated with powder q_e (method 1) and the other one estimated with granule q_e (method 2). The kinetic constants obtained at 250 mg/L dosage were used in the model.

When the powder isotherm was used, the Freundlich constant K_F should be scaled

down 85% to account for the bentonite fraction in the granules, and the method 1 kinetic constants obtained with powder q_e should be used. When the granule isotherm was used, it should always be combined with method 2 kinetic constants obtained with granule q_e. In short, three modelling scenarios can be formulated:

Scenario 1 : Powder isotherm * 0.85 + kinetic constants from powder q_e (Method 1)

Scenario 2: Full-sized granule isotherm + kinetic constants from granule q_e (Method 2)

Scenario 3: Pulverized granule isotherm + kinetic constants from granule q_e (Method 2)

Results for scenario 1, 2 and 3

With the isotherm and kinetic parameters in scenario 1, 2 and 3, together with the dispersion coefficients and the operating parameters, the breakthrough curves were simulated for BEA and MOR column at 6 min EBCT. The model results of scenario 1, 2 and 3 were presented in Figure 3.13.
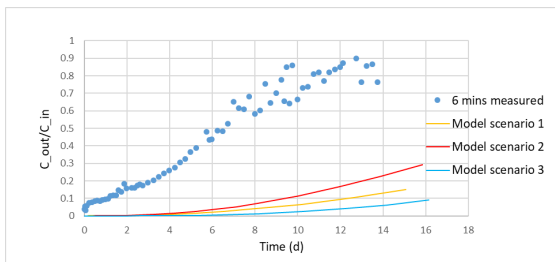
(a) Benzo. (BEA)
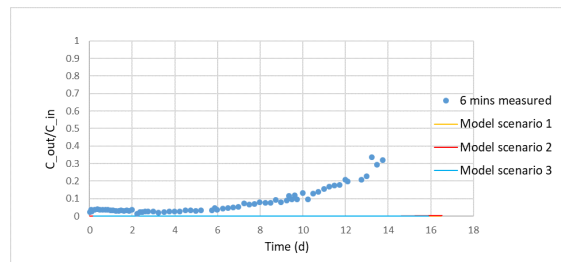
(b) Methyl-benzo. (BEA)
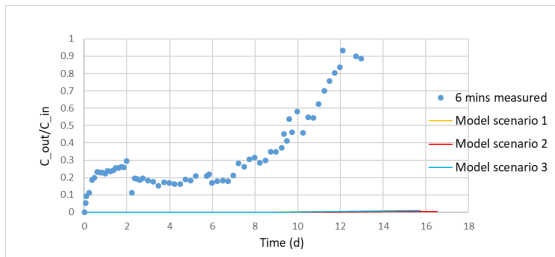
(c) Sulfa. (BEA)
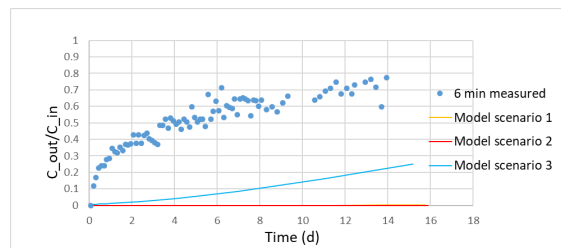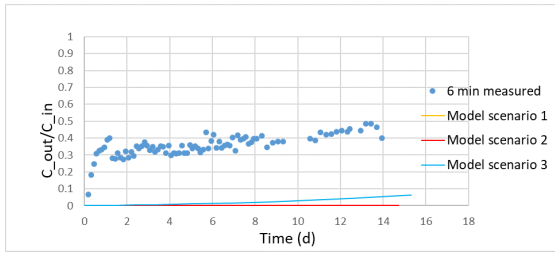
(d) Benzo. (MOR)

(e) Methyl-benzo. (MOR)
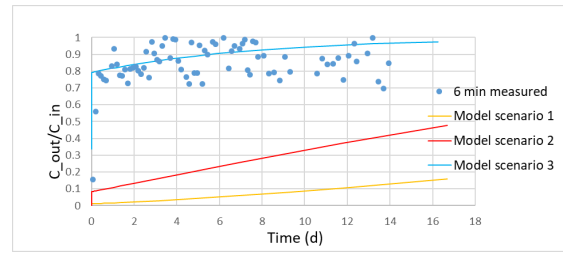
(f) Sulfa. (MOR)

Figure 3.13: OMP breakthrough curves modelled from scenario 1, 2 and 3 in comparison with experimental breakthrough curve at EBCT 6 min

As can be seen from the above graphs, except for sulfamethoxazole which had similar results to the real curve in scenario 3, other modelled curves were all far below the actual breakthrough curves. It means that the adsorption kinetics and/or capacities were overestimated with the parameters obtained in batch experiments. To solve the problem, kinetic and isotherm constants were adjusted individually to model the best fit curve.

Effect of kinetic constant on modelled breakthrough curve

According to the fact that slower adsorption kinetics of a compound leads to a faster breakthrough, a closer simulation result was expected by using a lower kinetic constant. The Method 2 kinetic constants were multiplied by 10%, 30%, 50% and were used to simulate the breakthrough curves at EBCT 6 min. Freundlich isotherm constants from powder zeolites was applied after scaling down to 0.85. The results were presented in Figure 3.14.

(a) Benzo. (BEA)
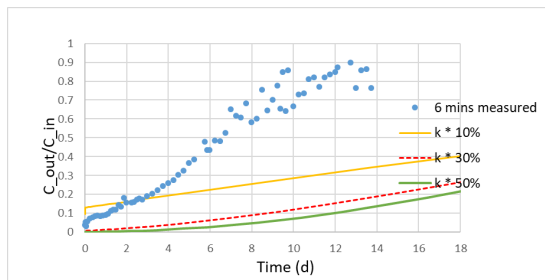
(b) Methyl-benzo. (BEA)
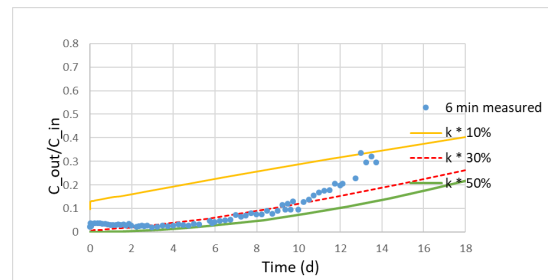
(c) Sulfa. (BEA)
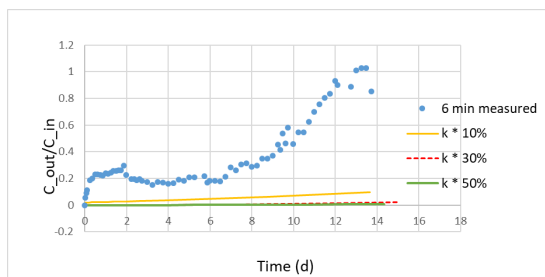
(d) Benzo. (MOR)
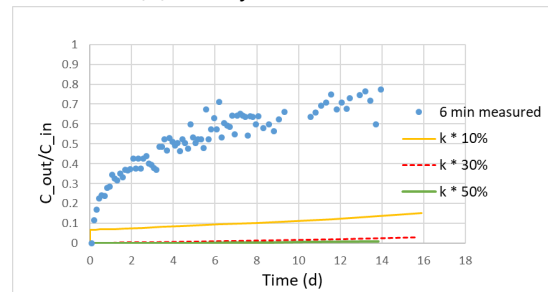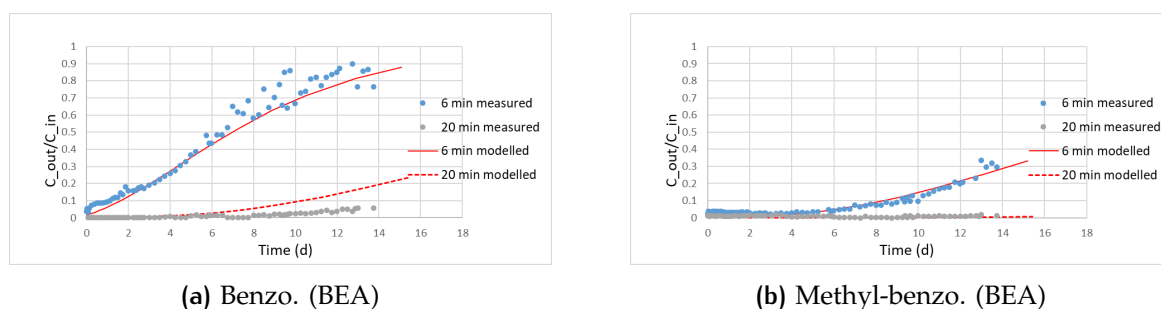
(e) Methyl-benzo. (MOR)   **(f)** Sulfa. (MOR)
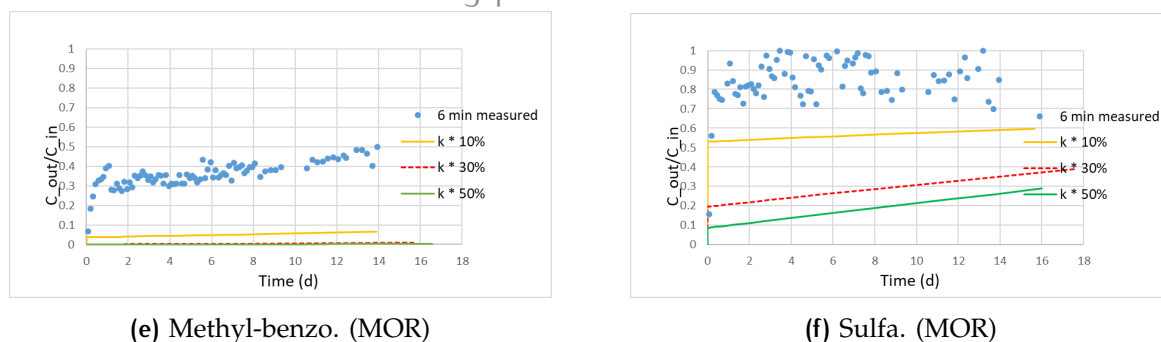
Figure 3.14: Modelled OMP breakthrough curves after applying lower kinetic constants in comparison with experimental breakthrough curve at EBCT 6 min

As shown in Figure 3.14, the lower kinetic constants didn't give better fittings to the experimental data. In most cases, the modelled curves were still below the experimental curves. Notably, the simulated curves with lower kinetic constants tended to breakthrough at the zero time point, and afterwards, the curves started to increase linearly. The shape of the modelled curves was somewhat similar to the actual breakthrough curves of the MOR column, especially for methyl-benzotriazole, which means that the kinetic constant might indeed be lower in the column than in the batch. However, since the one magnitude lower kinetic constants were already small values, a further decrease on these constants might not be reasonable. Therefore, the kinetic constant should not be the only parameter that was underestimated in batch experiments.

Effect of isotherm constant on modelled breakthrough curves

Zeolites tended to have linear isotherms for the adsorption of OMPs under low concentration. For simplicity, the linear isotherm was applied by fixing the n values in the Freundlich isotherm as one. By varying the values of K_L in the isotherms, the model results were adjusted to fit the experimental results. The optimum K_L that matched well with breakthrough curve at 6 min EBCT was determined. The kinetic constants were estimated by Method 2 at 250 mg/L zeolite dosage. Afterwards, the determined K_L together with corresponding operating parameters were used to simulate the breakthrough curves at 20 min EBCT (Figure 3.15). The K_L obtained from breakthrough models, together with powder and granule K_L obtained from batch experiments were compared in Table 3.11.
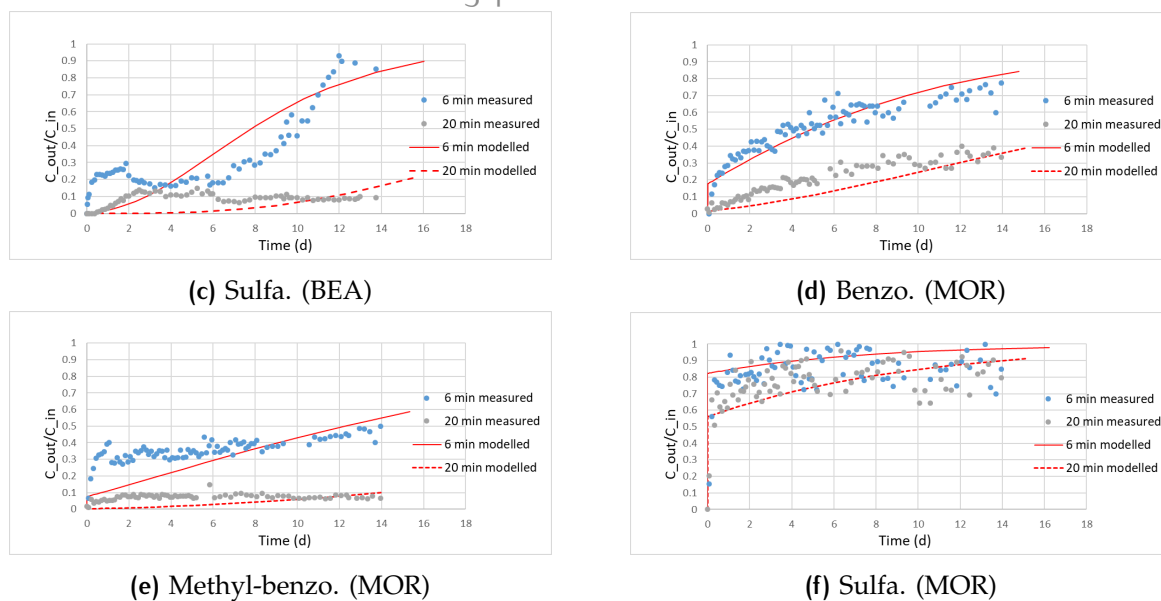

(a) Benzo. (BEA)   **(b)** Methyl-benzo. (BEA)

(c) Sulfa. (BEA)

(d) Benzo. (MOR)

(e) Methyl-benzo. (MOR)

(f) Sulfa. (MOR)

Figure 3.15: Modelling results with optimized linear isotherm constant K_L at EBCT 6 min

Table 3.11: The summarize of linear isotherm constants K_L [a]

	BEA			MOR		
	1H-Benzo.	Methyl-Benzo.	Sulfa.	1H-Benzo.	Methyl-Benzo.	Sulfa.
K_L for powder (*0.85)	5.1	43.4	11.2	15.0	102.9	17.5
K_L for full sized granule	4.3	11.8	7.7	24.3	36.2	8.9
K_L for pulverized granule	5.7	16.9	9.2	3.8	7.8	0.6
K_L from breakthrough model	1.2	3.2	1.2	2.8	6.1	0.5

[a] Unit of K_L: m^3/kg.

It was found in Figure 3.15 that adjusting K_L was a feasible way to obtain relatively good fittings. Therefore, the different isotherm constants in the batch and column experiments should be the main reasons which led to the deviation of the modelled curves. Furthermore, the determined K_L from the breakthrough curves at EBTC 6 min gave good predictions on the curves of 20 min.

As stated in Table 3.11, the K_L values determined from the breakthrough model at 6 min EBCT were lower than both the powder K_L and the granule K_L. Therefore, it was suggested that the real utilized adsorption capacity of the zeolite granules were lower under column conditions than under batch conditions.

Moreover, it can be noticed that the instantaneous increase of sulfamethoxazole and methyl-benzotriazole at zero time point in the experimental curves were not well simulated by a lower K_L, the overestimation on the kinetic constants of this two compounds from batch experiments might be responsible for this.

Possible reasons for the lower isotherm and kinetic constants

The different kinetic constants might be due to the different hydraulic conditions in the column and batch. Since the film diffusion cannot be ignored during the adsorption process, it can be assumed that a thicker water film might appear under column conditions, and it took more time for OMPs to diffuse into the water film and reach the adsorption sites on zeolite surface. Besides, despite the different kinetic constants in column and batch, the difference between the kinetic constants in the two columns at 6 min and 20 min EBCT was thought to be insignificant.

The possible reason for the lower adsorption capacity of OMPs under column conditions might be due to the shorter residence time of water in the column compared with batch. In the column, with limited residence time of water and lower kinetics of OMPs, the diffusion of OMPs into zeolite granules was hindered. Thus, the penetration depth of OMPs into the granules was smaller in the column than in the batch, which means that there was a larger amount of unused portion on the granules in the column. With the unused portion remained in the granules, it can be equal to the situation where the column was packed with less granules. However, the theoretical packing weight of zeolite granules was accounted in the breakthrough modelling, which resulted in an overestimation on the column performance by the model. Therefore, a lower K_L value can be used to correct for the overestimation on the granule packing weight.

3.4.3 Sensitivity analysis

The influences of D_L, granule bulk density, porosity, granule packing height and flow velocity were investigated for the breakthrough curves of 1H-benzotriazole at EBCT 6 min. The parameters of interest were varied by ±30% to check the sensitivity of the model to these parameters. The results are shown in Figure 3.16.
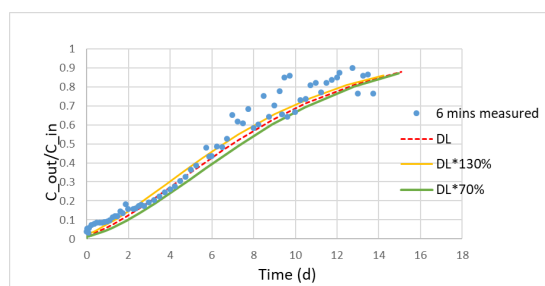
(a) Dispersion coefficient

(b) Bulk density (pho_b)

(c) Porosity (ep)

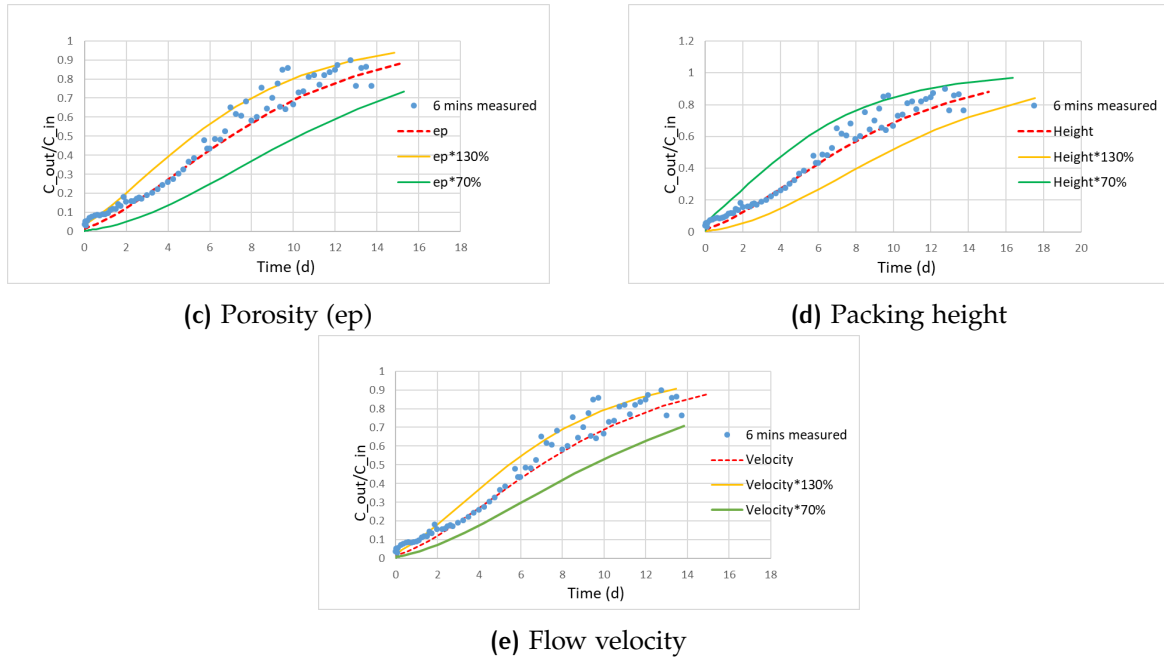

(d) Packing height

(e) Flow velocity
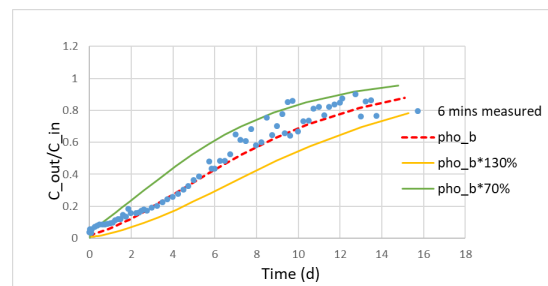
Figure 3.16: Sensitivity analysis

From the above graphs, it can be found that D_L had the minimal impact on the modelled breakthrough curves. The curve with a larger D_L showed a slightly faster breakthrough. Larger D_L gave smaller Peclet number, which meant advection was more dominant over diffusion in the system. This way, the OMP molecules flow with the water without enough time to diffuse into the water film surrounding the zeolite granules, resulting in the poor adsorption.

The ±30% change on bulk density, porosity and packing height all led to obvious deviation on the modelled curves, which means the proper determination of these parameters is of great importance in breakthrough modelling. It indicated that the underestimated (-30%) bulk density and packing height, and the overestimated (+30%) porosity gave faster breakthrough , which were due to the lower packing weight of zeolite granules.

Lastly, the breakthrough was faster with higher flow velocity. This was likely due to the reduced residence time of the target OMP in the column, and more OMP inputs during the same operating period. Therefore, the proper determination of this parameter was also of great importance.

4 | CONCLUSIONS

In this research, the application potential of zeolite granules to remove 11 target OMPs in demi-water and WW was investigated. Batch experiments were performed to study the adsorption isotherm and kinetics; the breakthrough of OMPs was studied in columns packed with zeolite granules. A model combining the isotherm and kinetics parameters was developed to predict the OMP breakthroughs in the column. The main conclusions of the research can be drawn:

- The adsorption capacity of the 11 OMPs by zeolite granules can be divided into three categories as shown in Table 4.1. The charge and hydrophobicity of OMPs were the two main factors that affected the adsorption capacity of OMPs by zeolites, while the effect of OMP size on the adsorption capacity can be neglected.

Table 4.1: Three categories of OMP removal capacity

Removal efficiency	Good removal	Medium removal	Bad removal
Name	Trimethoprim, metoprolol, propranolol, sotatol, clarithromycin	1H-benzotriazole, methyl-benzotriazole, sulfamethoxazole, hydrochlorothiazide	Carbamazepine, diclofenac

- The OMP adsorption capacities by zeolite granules were less than OMP adsorption capacities by zeolite powders. It was hypothesised that OMPs were more likely to be adsorbed on the external surface of zeolite granules instead of entering the inner pores.

- The fittings of the IPD model to the adsorption kinetic data showed that film diffusion and intra-particle diffusion were both the rate limiting steps in the adsorption of OMPs by zeolite granules.

- The adsorption capacity and rates of OMPs in WW were lower in comparison with OMP adsorption in demi-water. The higher pH of the WW and the pore-blocking effects by BOMs might be the main reason for the reduced capacity and kinetics.

- BEA columns had better performances than MOR columns under the same packing volume and operating conditions. The OMP breakthrough percentages in the column were determined by both the adsorption capacity and kinetics of the OMPs by zeolite granules. The breakthrough percentages of different OMPs with similar adsorption capacities were affected by the adsorption kinetics.

- The breakthrough model with the kinetic and isotherm constants determined by batch experiments, with both the powders as well as the granules, cannot make good predictions on the real breakthrough curve of the columns. It was found that both the kinetic and the isotherm constants were supposed to be lower in the column than those in the batch, while the isotherm constant was the main cause of the deviation on the model prediction. With a lower isotherm constant, the model was able to provide good resemblance between modelled and measured breakthrough curves. Furthermore, with a known breakthrough curve at a certain EBCT, the model was able to determine a proper isotherm constant, which can be used to make prediction on the breakthrough curve at a different EBCT.

5 | LIMITATIONS AND SUGGESTIONS

Based on the conducted experiments, the following suggestions are proposed to improve the current methodology and future research:

- For the experiment of adsorption isotherms in WW, zeolite dosages were from 1 mg/L to 1000 mg/L, however, the concentration decrease under low dosage, i.e. 1, 5 and 10 mg/L, was not obvious, which led to the poor quality of the isotherm fitting. Therefore, more dosages between the range of 50 mg/L and 1000 mg/L were suggested.

- Further research on the isotherm of zeolite granules was recommended. For example, the adsorption isotherms of full sized zeolite granules should be determined. Used full sized granules can be pulverized in order to measure the remained adsorption capacity of the granules.

- Packing more zeolites in the column will improve OMP adsorption efficiencies and meanwhile, will increase the expense of the column. Future research should be carried out on the balance between the OMP removal efficiency and the expense of the column, in order to find the optimum design that can minimize the cost. To compare OMP removal efficiency by different types of zeolite granules, a fixed weight of zeolites can be used instead of the fixed height of zeolites in the column experiments.

- In this study, the effect of kinetic constants and isotherm constants on the performances of the breakthrough model were studied separately, by fixing one and changing another one. It was recommended to investigate the scenario where the kinetic and isotherm constants are simultaneously performed as adjustable parameters to find out the proper constants for predicting the curves at another EBCT. However, the drawback of this approach is that there is a possibility that the wrong set of parameters is used in the calculations which should be carefully noted.

- Due to the outbreak of COVID-19, it was not allowed to collect WW samples since February 2020. As a result, the column experiment and breakthrough model in WW was not studied in this research. Compared with OMP adsorption in demi-water, the adsorption capacity of OMPs in WW was less and the adsorption rates in WW was lower. It can be speculated that there will be a

faster breakthrough of OMPs in WW. It was suggested to carry out column experiments in WW and to build up a model for the prediction of OMP breakthrough in WW.

BIBLIOGRAPHY

Abu-Lail, L., Bergendahl, J. A., and Thompson, R. W. (2010). Adsorption of methyl tertiary butyl ether on granular zeolites: Batch and column studies. *Journal of Hazardous Materials*, page 363–369.

Abu-Lail, L., Bergendahl, J. A., and Thompson, R. W. (2012). Mathematical modeling of chloroform adsorption onto fixed-bed columns of highly siliceous granular zeolites. *Environmental Progress & Sustainable Energy*, 31(4):591–596.

Acero, J. L. and Von Gunten, U. (2001). Characterization of oxidation processes: ozonation and the aop o3/h2o2. *Journal-American Water Works Association*, 93(10):90–100.

Alsbaiee, A., Smith, B. J., Xiao, L., Ling, Y., Helbling, D. E., and Dichtel, W. R. (2016). Rapid removal of organic micropollutants from water by a porous β-cyclodextrin polymer. *Nature*, page 190–194.

Auerbach, S. M., Carrado, K. A., and Dutta, P. K. (2003). *Handbook of zeolite science and technology*. CRC Press.

Baerlocher, C., McCusker, L. B., and Olson, D. H. (2007). *Atlas of zeolite framework types*. Elsevier.

Baresel, C., Harding, M., and Fang, J. (2019). Ultrafiltration/granulated active carbon-biofilter: Efficient removal of a broad range of micropollutants. *Applied science*. 9,710.

Blanchard, G., Maunaye, M., and Martin, G. (1984). Removal of heavy metals from waters by means of natural zeolites. *Water research*, 18:1501–1507.

Blasioli, S., Martucci, A., Paul, G., Gigli, L., Cossi, M., Johnston, C. T., Marchese, L., and Braschi, I. (2014). Removal of sulfamethoxazole sulfonamide antibiotic from water by high silica zeolites: a study of the involved host–guest interactions by a combined structural, spectroscopic, and computational approach. *Journal of colloid and interface science*, 419:148–159.

Boyd, G., Adamson, A., and Myers Jr, L. (1947). The exchange adsorption of ions from aqueous solutions by organic zeolites. ii. kinetics1. *Journal of the American Chemical Society*, 69(11):2836–2848.

Castiglioni, S., Bagnati, R., Fanelli, R., Pomati, F., Calamari, D., and Zuccato, E. (2006). Removal of pharmaceuticals in sewage treatment plants in italy. *Environmental science & technology*, 40(1):357–363.

Castilla, C. M. (2004). Adsorption of organic molecules from aqueous solutions on carbon materials. *Carbon*, 42:83–94.

Chiron, S., Fernandez-Alba, A., Rodriguez, A., and Garcia-Calvo, E. (2000). Pesticide chemical oxidation: state-of-the-art. *Water Research*, pages 366–377.

Chu, K. H. (2010). Fixed bed sorption: setting the record straight on the bohart–adams and thomas models. *Journal of Hazardous Materials*, 177(1-3):1006–1012.

Clara, M., Strenn, B., Gans, O., Martinez, E., Kreuzinger, N., and Kroiss, H. (2005). Removal of selected pharmaceuticals, fragrances and endocrine disrupting compounds in a membrane bioreactor and conventional wastewater treatment plants. *Water Research*, 39:4797–4807.

Damjanovi´, c, L., Raki´c, V., Rac, V., Stoši´c, D., and Auroux, A. (2010). The investigation of phenol removal from aqueous solutions by zeolites as solid adsorbents. *Journal of Hazardous Materials*, 184:477–484.

Damjanovi´c, L., Raki´c, V., Racb, V., ´c, D. S., and Auroux, A. (2010). The investigation of phenol removal from aqueous solutions by zeolites as solid adsorbents. *Journal of Hazardous Materials*, pages 477–484.

De Ridder, D. J., Verberk, J., Heijman, S. G., Amy, G. L., and Van Dijk, J. C. (2012). Zeolites for nitrosamine and pharmaceutical removal from demineralised and surface water: mechanisms and efficacy. *Separation and purification technology*, 89:71–77.

Foster, M., Rivin, I., Treacy, M., and Friedrichs, O. D. (2006). A geometric solution to the largest-free-sphere problem in zeolite frameworks. *Microporous and mesoporous materials*, 90(1-3):32–38.

Freundlich, H. (1906). *Über die absorption in lösungen. Über Die Adsorption in Lösungen.*

Furusawa, T. and Smith, J. (1973). Fluid-particle and intraparticle mass transport rates in slurries. *Industrial & Engineering Chemistry Fundamentals*, 12(2):197–203.

Gavrilescu, M., Demnerová, K., Aamand, J., Agathos, S., and Fava, F. (2015). Emerging pollutants in the environment: present and future challenges in biomonitoring, ecological risks and bioremediation. *New Biotechnologyl Environment*, pages 147–156.

Giles, C. H., Smith, D., and Huitson, A. (1974). A general treatment and classification of the solute adsorption isotherm. i. theoretical. *Journal of colloid and interface science*, 47(3):755–765.

Göbel, A., McArdell, C. S., Joss, A., Siegrist, H., and Giger, W. (2007). Fate of sulfonamides, macrolides, and trimethoprim in different wastewater treatment technologies. *Science of the Total Environment*, 372(2-3):361–371.

Halder, G., Khan, A., and Dhawane, S. (2016). Fluoride sorption onto a steam-activated biochar derived from cocos nucifera shell. *CLEAN Soil Air Water*, 44:124–133.

Hameed, B. and El-Khaiary, M. (2008). Batch removal of malachite green from aqueous solutions by adsorption on oil palm trunk fibre: equilibrium isotherms and kinetic studies. *Journal of hazardous materials*, 154(1-3):237–244.

Han, R., Ding, D., Xu, Y., Zou, W., Wang, Y., Li, Y., and Zou, L. (2008). Use of rice husk for the adsorption of congo red from aqueous solution in column mode. *Bioresource technology*, 99(8):2938–2946.

Heijman, S., Siegers, W., Sterk, R., and Hopman, R. (2002). Prediction of breakthrough of pesticides in gac-filters and breakthrough of colour in ion-exchange-filters. *Water Science and Technology: Water Supply*, 2:103–108.

Helfferich, F. (1984). Principles of adsorption & adsorption processes, by d. m. ruthven, john wiley & sons. *AIChE J*, 31:523–524.

Ho, Y. and Chiang, C. (2001). Sorption studies of acid dye by mixed sorbents. *Adsorption*, 7(2):139–147.

Jiang, N. (2019). High-silica zeolites as novel adsorbents for the removal of organic micro-pollutants in water treatment.

Jiang, N., Erdős, M., Moultos, O. A., Shang, R., Vlugt, T. J., Heijman, S. G., and Rietveld, L. C. (2020). The adsorption mechanisms of organic micropollutants on high-silica zeolites causing s-shaped adsorption isotherms: An experimental and monte carlo simulation study. *Chemical Engineering Journal*, 389:123968.

Jiang, N., Shang, R., Heijman, S. G., and Rietveld, L. C. (2018). High-silica zeolites for adsorption of organic micro-pollutants in water treatment: A review. *Water Research*, pages 145–161.

Kalavathy, M. H., Karthikeyan, T., Rajgopal, S., and Miranda, L. R. (2005). Kinetic and isotherm studies of cu (ii) adsorption onto h3po4-activated rubber wood sawdust. *Journal of colloid and interface science*, 292(2):354–362.

Katsoyiannis, I. A., Canonica, S., and von Gunten, U. (2011). Efficiency and energy requirements for the transformation of organic micropollutants by ozone, o3/h2o2 and uv/h2o2. *Water research*, 45(13):3811–3822.

Kimura, K., Amy, G., Drewes, J. E., Heberer, T., Kim, T.-U., and Watanabe, Y. (2003). Rejection of organic micropollutants (disinfection by-products, endocrine disrupting compounds, and pharmaceutically active compounds) by nf/ro membranes. *Journal of Membrane Science*, pages 113–121.

Koubaissy, B., Joly, G., Batonneau-Gener, I., and Magnoux, P. (2011). Adsorptive removal of aromatic compounds present in wastewater by using dealuminated faujasite zeolite. *Industrial Engineering Chemistry Research*, pages 5705–5713.

Kruithof, J. C., Kamp, P. C., and Martijn, B. J. (2006). Uv/h2o2 treatment: A practical solution for organic contaminant control and primary disinfection. *Ozone: Science Engineering*, pages 273–280.

Lagergren, S. (1898). About the theory of so-called adsorption of soluble substances. *Kungliga Svenska Vetenskapsakademiens Handlingar*, 24:1–39.

Langmuir, I. (1916). The constitution and fundamental properties of solids and liquids. part i. solids. *Journal of the American Chemical Society*, 38:2221–2295.

Laîné, J. M., Campos, C., I., B., and Janex, M. L. (2003). Understanding membrane fouling: A review of over a decade of research. *Water Science and Technology: Water Supply*, page 155–164.

Leung, C. S., Leung, S. S., and Tirado-Rives, J.and Jorgensen, W. L. (2012). Methyl effects on protein–ligand binding. *Journal of medicinal chemistry*, 55:4489–4500.

Li, Y. and Yu, J. (2014). New stories of zeolite structures: Their descriptions, determinations, predictions, and evaluations. *Chemical reviews*, page 72687316.

Limousin, G., Gaudet, J.-P., Charlet, L., Szenknect, S., Barthes, V., and Krimissa, M. (2007). Sorption isotherms: A review on physical bases, modeling and measurement. *Applied geochemistry*, 22(2):249–275.

Loos, R., Carvalho, R., Anto´nio, D. C., Comero, S., Locoro, G., Tavazzi, S., Paracchini, B., Ghiani, M., Lettieri, T., Blaha, L., Jarosova, B., Voorspoels, S., Servaes, K., Haglund, P., Fick, J., Lindberg, R. H., Schwesig, D., and Gawlik, B. M. (2013). Eu-wide monitoring survey on emerging polar organic contaminants in wastewater treatment plant effluents. *Water research*, 47:6475–6487.

Luo, Y., Guo, W., Ngo, H., Nghiem, L., Hai, F. I., Zhang, J., Liang, S., and Wang, X. C. (2014). A review on the occurrence of micropollutants in the aquatic environment and their fate and removal during wastewater treatment. *Science of the Total Environment*, pages 619–641.

Marta, O. B., Moreira, N. F., Ribeiro, A. R., Pereira, M. F., and Silva, A. M. (2016). Occurrence and removal of organic micropollutants: An overview of the watch list of eu decision 2015/495. *Water Research*, 94:257–279.

Martucci, A., Pasti, L., Marchetti, N., Cavazzini, A., Dondi, F., and Alberti, A. (2012). Adsorption of pharmaceuticals from aqueous solutions on synthetic zeolites. *Microporous and Mesoporous Materials*, 148(1):174–183.

Maurer, M., Escher, B., Richle, P., Schaffner, C., and Alder, A. (2007). Elimination of b-blockers in sewage treatment plants. *Water Research*, 41:1614–1622.

McKay, G., Otterburn, M. S., and Aga, J. A. (1985). Fuller's earth and fired clay as adsorbents for dyestuffs. *Water, Air, and Soil Pollution*, 24(3):307–322.

Mohammad-Khah, A. and Ansari, R. (2009). Activated charcoal: preparation, characterization and applications: a review article. *Int J Chem Tech Res*, 1(4):859–864.

Oosterhuis, M., Sacher, F., and ter Laak, T. L. (2013). Prediction of concentration levels of metformin and other high consumption pharmaceuticals in wastewater and regional surface water based on sales data. *Science of the Total Environment*, 442:380–388.

Redlich, O. and Peterson, D. L. (1959). A useful adsorption isotherm. *Journal of physical chemistry*, 63(6):1024–1024.

Rossner, A. and Knappe, D. R. (2008). Mtbe adsorption on alternative adsorbents and packed bed adsorber performance. *Water Research*, pages 2287–2299.

Rossner, A., Snyder, S. A., and Knappe, D. R. (2009). Removal of emerging contaminants of concern by alternative adsorbents. *Water research*, 43(15):3787–3796.

Rungsirisakun, R., Nanok, T., Probst, M., and Limtrakul, J. (2006). Adsorption and diffusion of benzene in the nanoporous catalysts fau, zsm-5 and mcm-22: A molecular dynamics study. *Journal of Molecular Graphics and Modelling*, 24(5):373–382.

San Miguel, G., Lambert, S., and Graham, N. (2001). The regeneration of field-spent granular-activated carbons. *Water Research*, 35(11):2740–2748.

Sharma, P., Hussain, N., Borah, D., and Das, M. (2013). Kinetics and adsorption behavior of the methyl blue at the graphene oxide/reduced graphene oxide nanosheetewater interface: a comparative study. *Journal of Chemical Engineering Data*, 58:3477–3488.

Sips, R. (1948). On the structure of a catalyst surface. *The Journal of Chemical Physics*, 16(5):490–495.

Squire, D. (2000). Reverse osmosis concentrate disposal in the uk. *Desalination*, 132(1-3):47–54.

Swaim, P., Royce, A., Smith, T., Maloney, T., Ehlen, D., and Carter, B. (2008). Effectiveness of uv advanced oxidation for destruction of micro-pollutants. *Ozone: Science Engineering*, pages 34–42.

Szabová, P., Hencelová, K., Sameliaková, Z., Marcová, T., Staňová, A. V., Grabicová, K., and Bodík, I. (2020). Ozonation: effective way for removal of pharmaceuticals from wastewater. *Monatshefte für Chemie-Chemical Monthly*, pages 1–7.

Tran, H. N., You, S.-J., Hosseini-Bandegharaei, A., and Chao, H.-P. (2017). Mistakes and inconsistencies regarding adsorption of contaminants from aqueous solutions: a critical review. *Water research*, 120:88–116.

Tröger, R., löckner, P., LutzAhrens, and KarinWiberg (2018). Micropollutants in drinking water from source to tap-method development and application of a multiresidue screening method. *Science of the Total Environment*, 627:1404–1432.

Tsai, W.-T., Hsu, H.-C., Su, T.-Y., Lin, K.-Y., and Lin, C.-M. (2006). Adsorption characteristics of bisphenol-a in aqueous solutions onto hydrophobic zeolite. *Journal of colloid and interface science*, 299(2):513–519.

Tsitsishvili, G. (1973). Physicochemical properties of high silica l and clinoptilolite zeolites. ACS Publications.

Valdés, H., amd Víctor A. Solar, Cabrera, E. H., Veloso, A. F., and Zaror, C. A. (2014). Control of released volatile organic compounds from industrial facilities using natural and acid-treated mordenites: The role of acidic surface sites on the adsorption mechanism. *Chemical Engineering Journal*, 244:117–127.

Wang, J. and Guo, X. (2020). Adsorption kinetic models: Physical meanings, applications, and solving methods. *Journal of Hazardous Materials*, 390:122156.

Weber, W. and Morris, J. (1963). Kinetics of adsorption carbon from solutions. *Journal Sanitary Engeering Division Proceedings*, 89:31–60.

Wu, F.-C., Tseng, R.-L., and Juang, R.-S. (2005). Comparisons of porous and adsorption properties of carbons activated by steam and koh. *Journal of Colloid and Interface Science*, 283(1):49–56.

Xu, P., Drewes, J. E., Kimb, T.-U., Bellona, C., and Amy, G. (2006). Effect of membrane fouling on transport of organic contaminants in nf/ro membrane applications. *Journal of Membrane Science*, page 165–175.

Xu, Z., Cai, J., and Pan, B. (2013). About the theory of so-called adsorption of soluble substances. *Zhejiang Univ. Sci*, A 14:155–176.

Yusuff, A., Popoola, L., Omitola, O., Adeodu, A., and Daniyan, I. (2013). Mathematical modelling of fixed bed adsorption column for liquid phase solute: effect of operating variables. *International Journal of Scientific & Engineering Research*, 4(8):811–822.

Zhang, Y., Jin, F., Shen, Z., Wang, F., Rod, L., and Al-Tabbaa, A. (2019). Adsorption of methyl tert-butyl ether (mtbe) onto zsm-5 zeolite: Fixed-bed column tests, breakthrough curve modelling and regeneration. *Chemosphere*, 220:422–431.

Zhang, Y., Prigent, B., and Geißen, S.-U. (2016). Adsorption and regenerative oxidation of trichlorophenol with synthetic zeolite: Ozone dosage and its influence on adsorption performance. *Chemosphere*, 154:132–137.

A | APPENDIX: CHEMICAL STRUCTURE OF OMP MOLECULES

(a) Benzotriazole
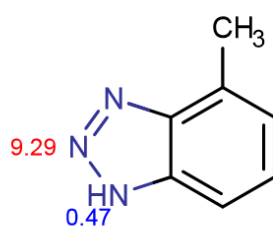
(b) Methyl-Benzotriazole
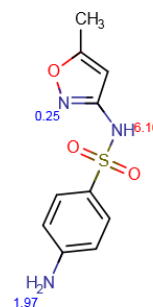
(c) Sulfamethoxazole
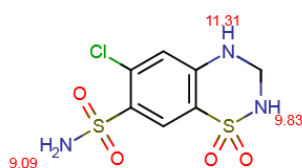
(d) Hydrochlorothiazide
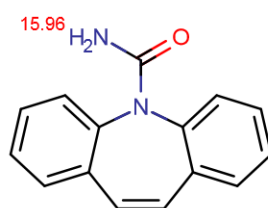
(e) Carbamazepine
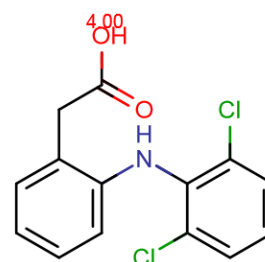
(f) Diclofenac
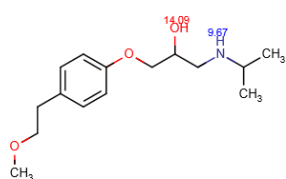
(g) Metoprolol
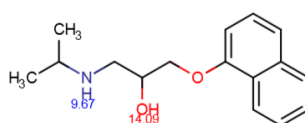
(h) Propranolol
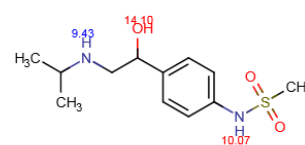
(i) Sotatol
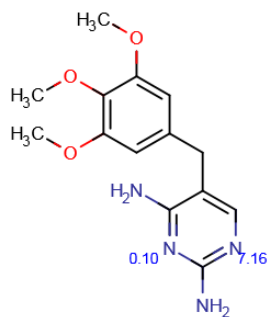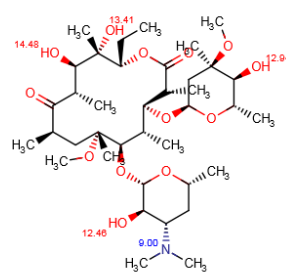
(j) Trimethoprim **(k)** Clarithromycin

Figure A.1: Chemical structure of OMPs (The numbers marked on the structures are the pKa values for each functional group)

B | APPENDIX: OMP ADSORPTION ISOTHERMS IN DEMI-WATER BY BEA AND MOR POWDERS WITH EQUILIBRIUM TIME OF 24H AND 48H.
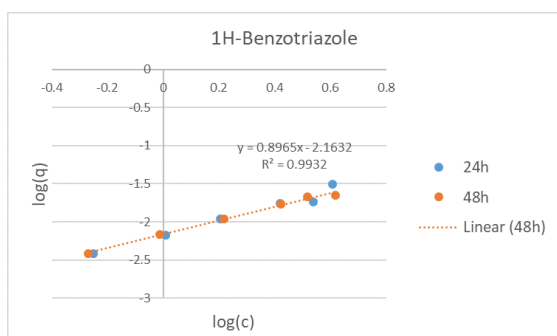
(a) BEA.
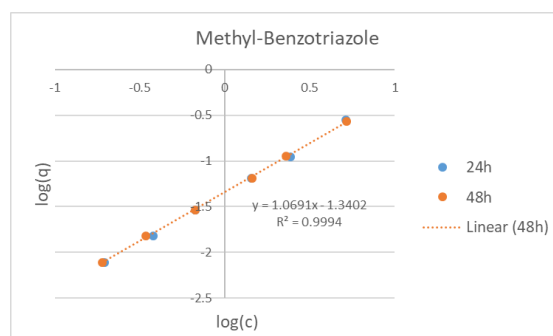
(b) BEA
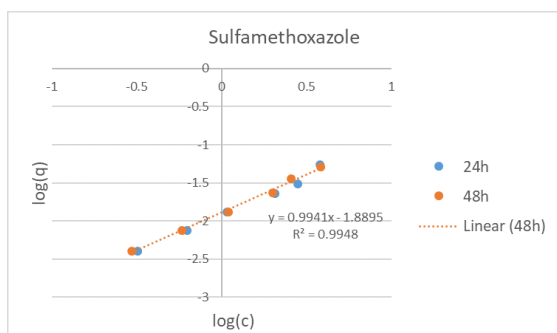
(c) BEA
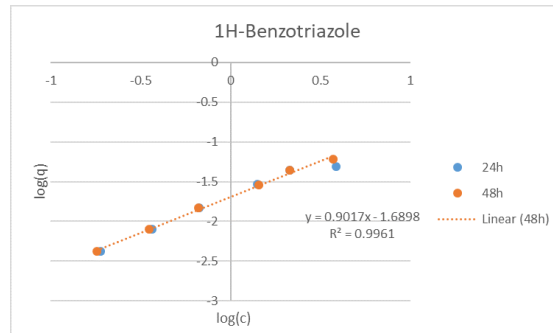
(d) MOR
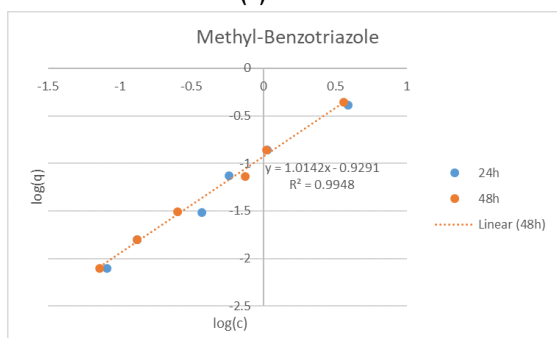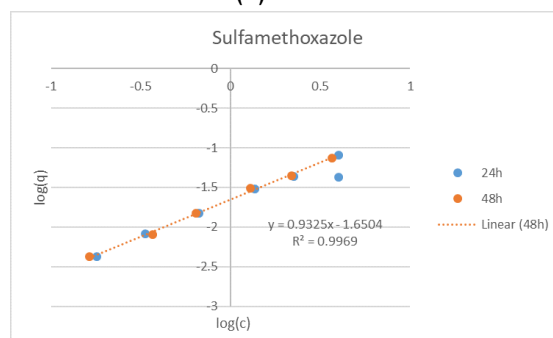
(e) MOR

(f) MOR

Figure B.1: Demi-water isotherms after 24 hours and 48 hours

APPENDIX: OMP ADSORPTION ISOTHERMS IN WW BY BEA AND MOR POWDERS WITH EQUILIBRIUM TIME OF 2D AND 8D.
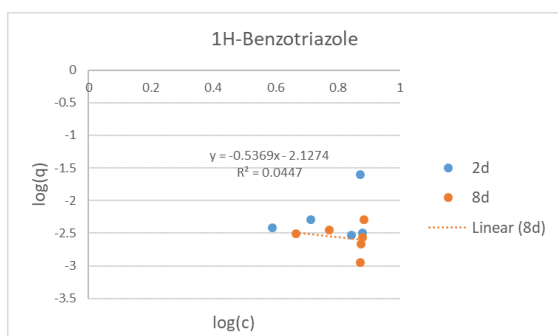
(a) BEA.
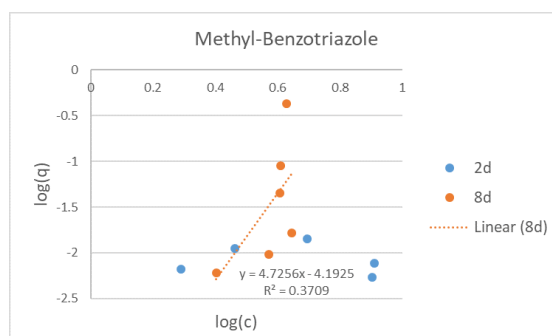
(b) BEA
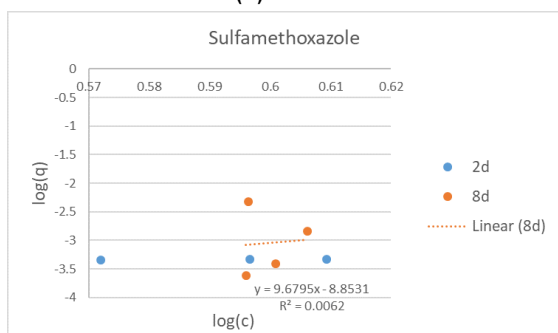
(c) BEA
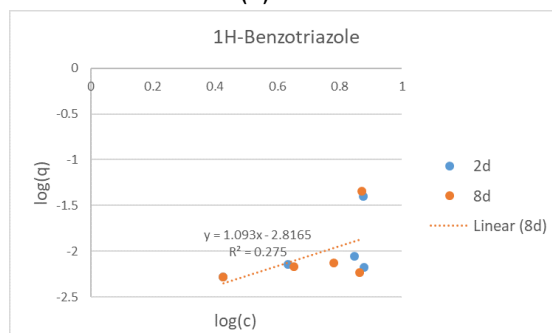
(d) MOR
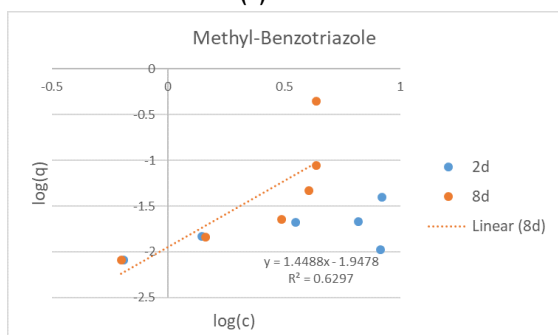
(e) MOR
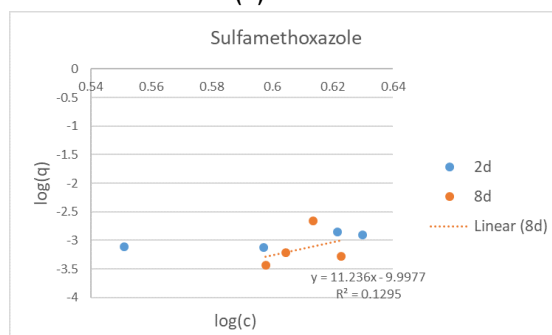
(f) MOR

Figure C.1: WW isotherms after 2d and 8d

APPENDIX: PFO FITTING FOR OMP ADSORPTION IN DEMI-WATER BY BEA AND MOR GRANULES
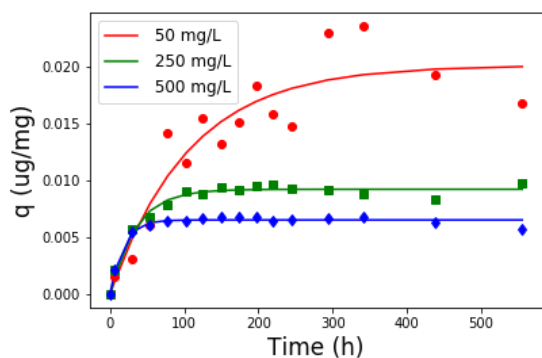
(a) 1H-Benzo.
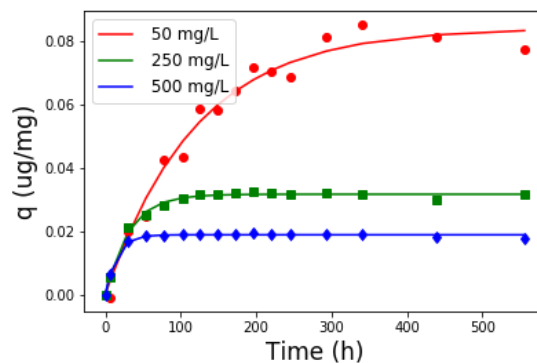
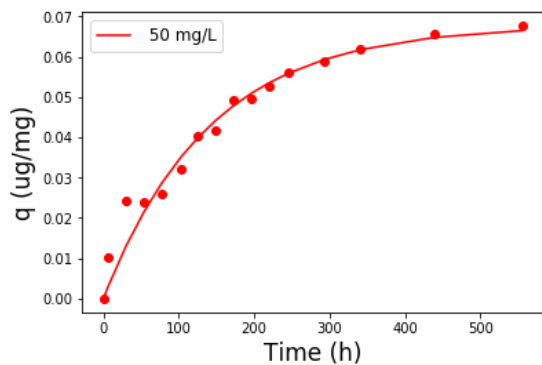**(b)** Methyl-Benzo.
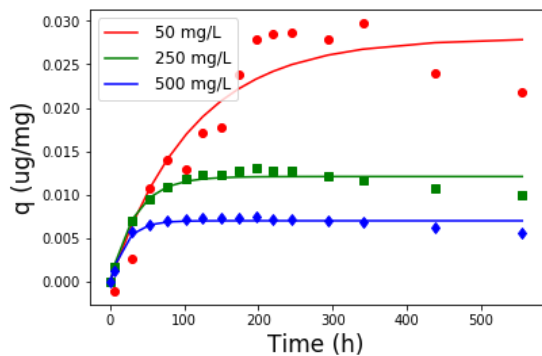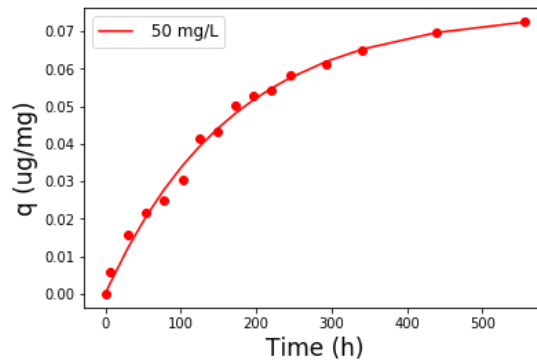
(c) Sulfa.
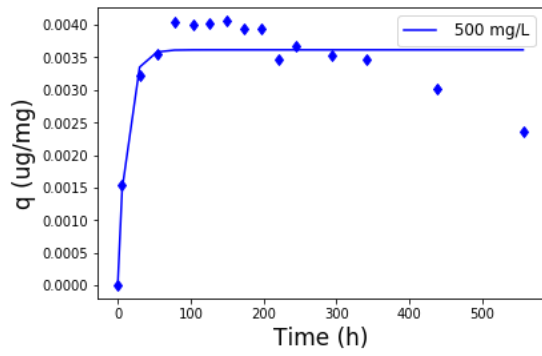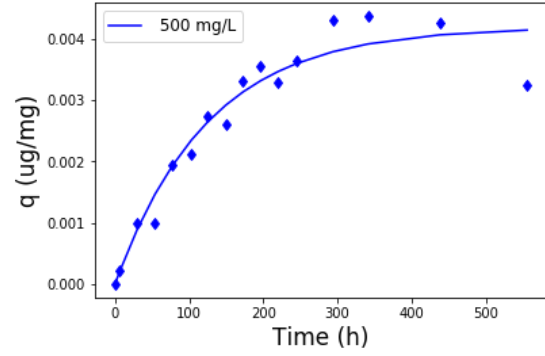

(d) Trime.
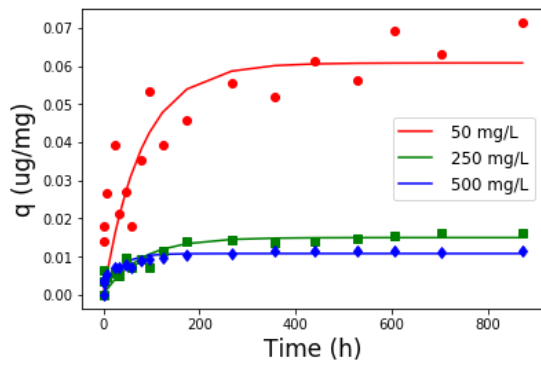

(e) Sotalol.
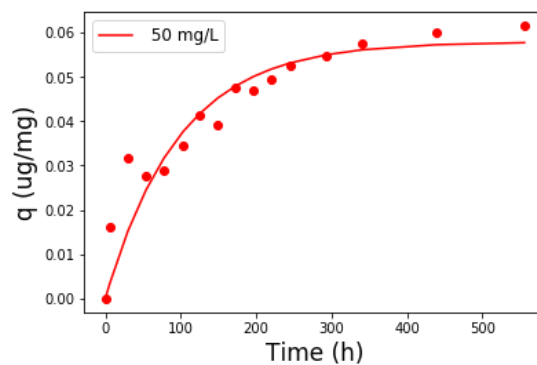
(f) Metop.

(g) Carba.

(h) Diclo.

Figure D.1: PFO fitting for OMP adsorption in demi-water by BEA granules (dots represent the experimental data, curves are the model fitting)

(a) 1H-Benzo.

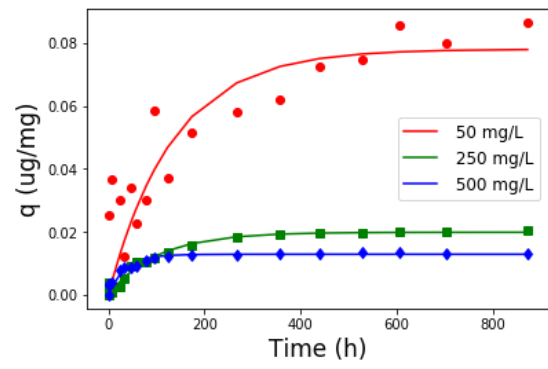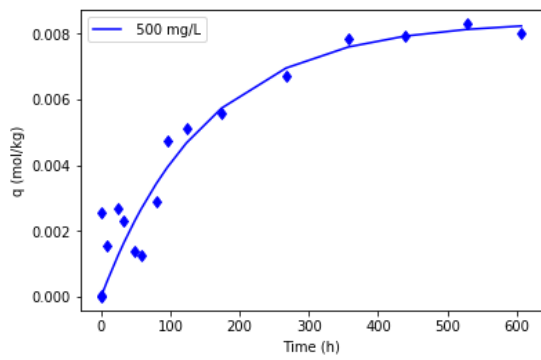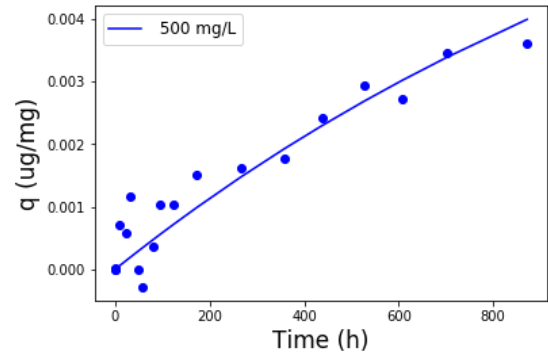(b) Methyl-Benzo.

(c) Sulfa.

(d) Carba.
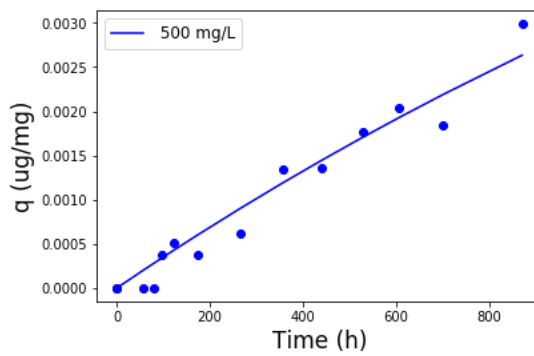
(e) Diclo.

Figure D.2: PFO fitting for OMP adsorption in demi-water by MOR granules (dots represent the experimental data, curves are the model fitting)

(a) 1H-Benzo.

(b) Methyl-Benzo.

(c) Sulfa.

(d) Carba.
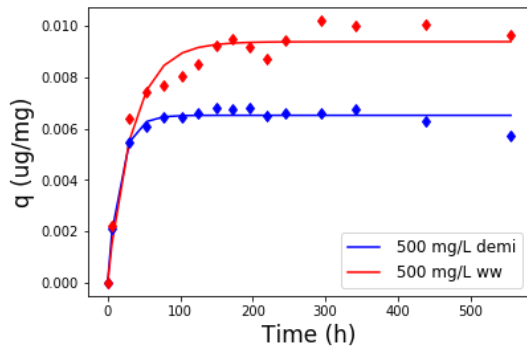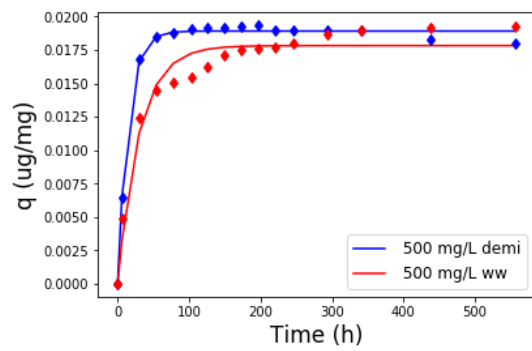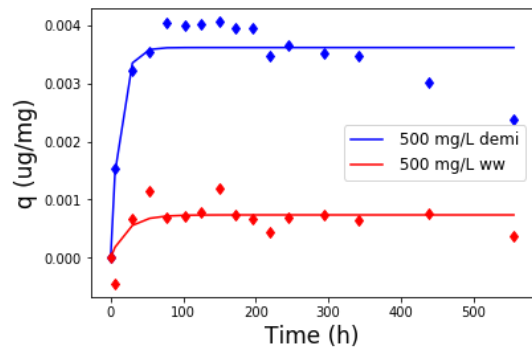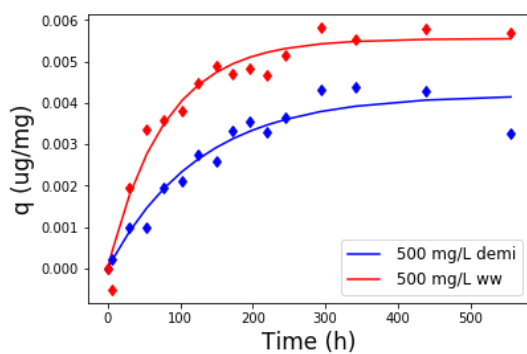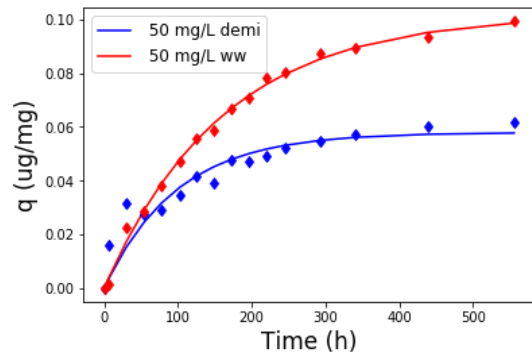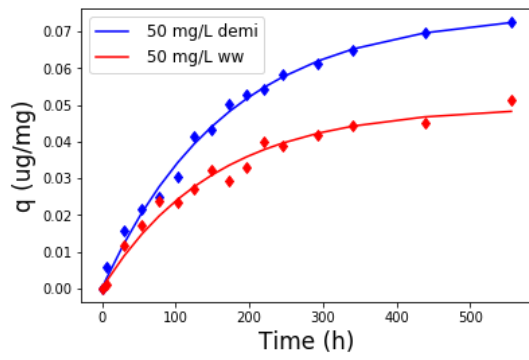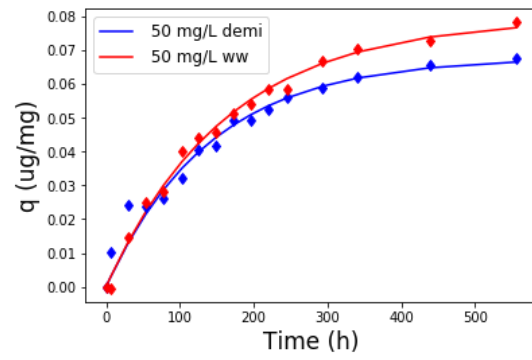
(e) Diclo.

(f) Metop.

(g) Trime.

(h) Sotalol.

Figure E.1: PFO fitting for OMP adsorption in demi-water and WW by BEA granules (dosage of 500 mg/L for medium-removal and bad-removal OMPs; dosage of 50 mg/L for good-removal OMPs)

F | APPENDIX: PREPARATION OF CALIBRATION STANDARDS FOR LC-MS

Table F.1: General preparation guide for standard samples in LC-MS

	Name	Concentration [µg/L]	Volume [µL]
Step 0 a	"single substance stock 0"	10000	1000
Step 0 b	"single iStd. stock"	10000	1000
Step 1	"iStd. Mix"	100	1500
Step 2	"stock 1"	50	1000
Step 3	"stock 2"	0.5	500

Table F.2: Detailed preparation guide for standard samples in LC-MS

iStd. Mix	Stock 1	Stock 2	Samples
total V [µL]	total V [µL]	total V [µL]	total V [µL]
1500	1000	500	500
target conc. [µg/L]	target conc. [µg/L]	target conc [µg/L]	iStd. Target conc. [µg/L]
100	50	0.5	1
single iStd. stock conc. [µg/L]	single subst. stock 0 conc. [µg/L]	stock 1 concentration [µg/L]	iStd. Mix concentration
10000	10000	50	100
stock V to add (per iStd.) [µL]	stock V to add (per subst.) [µL]	stock 1 V to add [µL]	iStd. Mix V to add [µL]
15	5	5	5
Number of iStds	Number of substances	-	-
10	22	-	-
V Elga to add [µL]	V Elga to add [µL]	V Elga to add [µL]	V sample to add [µL]
1350	890	495	495

Table F.3: Detailed preparation guide for calibration standards in LC-MS

target volume [µL]				
1000				
	iStd. target conc. [µg/L]			
	1			
stock name =>	iStd. Mix	stock 1	stock 2	ELGA water
stock conc. [µg/L] =>	100	50	0.5	-
cali. stand. target conc. [µg/L]	V to add [µL]	V to add [µL]	V to add [µL]	V to add [µL]
0	10		0	990
0.0025	10		5	985
0.005	10		10	980
0.01	10		20	970
0.05	10		100	890
0.1	10		200	790
0.5	10	10		980
1	10	20		970
2.5	10	50		940
5	10	100		890
10	10	200		790
Sequence of addition =>	iStd. Mix: 1st	stock: 3rd	stock: 3rd	ELGA water: 2nd

APPENDIX: THE INFORMATION OF OMP STANDARDS AND INTERNAL STANDARDS FOR LC–MS

Table G.1: The information of OMP standards and internal standards for LC-MS

Substance	CAS numbers		Molecular weights			purity	Manufact./Supplier
	standard	actual analyte	standard (salt, ...)	actual analyte	monoisotopic		
[name]			[g/mol]	[g/mol]	[Da]	[%]	
Benzotriazole	95-14-7	95-14-7	119.127	119.127	119.048	100.0	
1H-Benzotriazole-4,5,6,7-d4	1185072-03-0	1185072-03-0	123.15	123.15	123.074	98.8	CDN Isotopes
Carbamazepine	298-46-4	298-46-4	236.269	236.269	236.095	99.0	Sigma-Aldrich
Carbamazepine-d8(Major)	N/A	N/A	244.32	244.32	244.145	97.8	TRC / Biozol
Clarithromycin	81103-11-9	81103-11-9	747.95	747.95	747.477	98.0	Sigma-Aldrich
Clarithromycin-N-methyl-d3	N/A	N/A	750.97	750.97	750.496	96.8	TRC / Biozol
Diclofenac Na	15307-79-6	15307-86-5	318.13	296.15	295.017	99.9	Sigma-Aldrich
Diclofenac Na hydrate-C6	1261393-73-0	N/A	405.16	302.11	301.037	97.0	Sigma-Aldrich
Hydrochlorothiazide	58-93-5	58-93-5	297.739	297.739	296.965	99.7	Sigma-Aldrich
Hydrochlorothiazide-3,3-d2	1219798-89-6	1219798-89-6	299.75	299.75	298.977	96.7	CDN Isotopes
4-Methyl-1H-benzotriazole	29878-31-7	29878-31-7	133.151	133.151	133.064	90.0	Sigma-Aldrich
5-Methyl-1H-benzotriazole	136-85-6	136-85-6	133.151	133.151	133.064	98.0	Sigma-Aldrich
5-Methyl-1H-benzotriazole-d6	1246820-65-4	N/A	139.19	139.19	139.1	91.4	TRC / Biozol
Metoprolol * (Tartrate)0.5	56392-17-7	51384-51-1	342.405	267.369	267.183	98.0	Sigma-Aldrich
Metoprolol-D7 HCl	1219798-61-4	N/A	310.87	274.41	274.227	96.5	TRC / Biozol
Propranolol HCl	318-98-9	525-66-6	295.804	259.343	259.157	99.0	Sigma-Aldrich
Propranolol HCl d7	1613439-56-7	N/A	302.85	266.387	266.201	97.0	Sigma-Aldrich
Sotalol HCl	959-24-0	3930-20-9	308.82	272.3638	272.1195	98.0	TLC/Sigma-Aldrich
Sotalol HCl d6	1246820-85-8	1246912-17-3	314.862	278.4	278.157		
Sulfamethoxazole	723-46-6	723-46-6	253.278	253.278	253.052	99.8	Sigma-Aldrich
Sulfamethoxazole-d4	1020719-86-1	1020719-86-1	257.3	257.3	257.077	97.9	CDN Isotopes
Trimethoprim	738-70-5	738-70-5	290.318	290.318	290.138	99.9	Sigma-Aldrich
Trimethoprim-d9	1189460-62-5		299.37	299.37		97.8	Sigma-Aldrich

H APPENDIX: MS PARAMETERS AND QUANTIFICATION IONS

Table H.1: MS parameters and quantification ions

Substance	MS cap	cone	ESI	mother	1		2	
[name]	[kV]	[V]	[+/-]	[Da]	[Da]	[V]	[Da]	[V]
Benzotriazole	0.5	70	+	120	64.95	15	91.95	11
1H-Benzotriazole-4,5,6,7-d4	0.5	50	+	124	69	18	95.95	15
Carbamazepine	-	40	+	237.1	179.05	34	194.05	18
Carbamazepine-d8(Major)	1	40	+	245.1	185.1	35	202.1	18
Clarithromycin	1.4	40	+	748.5	158.2	28	590.4	18
Clarithromycin-N-methyl-d3	1.7	40	+	751.5	161.2	28	593.5	18
Diclofenac Na		20	+	296.05	214	35	215	20
Diclofenac Na hydrate-C6	0.5	20	+	302.1	171	17	221.1	16
Hydrochlorothiazide	0.7	20	-	295.95	205	21	268.95	18
Hydrochlorothiazide-3,3-d2	0.5	55	-	298	206	20	269.95	17
5-Methyl-1H-benzotriazole	0.8	50	+	124	69	18	95.95	15
5-Methyl-1H-benzotriazole-d6		50	+	134.05	77	22	79	16
Metoprolol * (Tartrate)0.5	0.8	40	+	268.2	72.05	20	116.05	18
Metoprolol-D7 HCl	1.7	40	+	275.25	79.15	25	123.1	20
Propranolol HCl	0.5	40	+	260.1	116	15	183.1	17
Propranolol HCl d7	0.5	40	+	267.2	123.1	16	105.1	17
Sotalol HCl	0.5	40	+	273.2	133.1	26	106.1	38
Sotalol HCl d6	0.5	40	+	279.3	214.3	17	182.4	19
Sulfamethoxazole		35	+	254.1	108	24	156	16
Sulfamethoxazole-d4	2	35	+	258.1	112.05	24	160.1	15
Trimethoprim	1.3	40	+	291.15	230.15	22	261.15	24
Trimethoprim-d9	0.5	47	+	300.2	234.3	25	264.3	25